# Augmenting Hypothermia Therapy for Hypoxic-Ischemic Encephalopathy in Neonates: Localizing Drug Delivery using pH and Temperature Responsive Nanoparticles

by

Rukhmani Narayanamurthy

A thesis submitted in partial fulfillment of the requirements for the degree of

Master of Science

Medical Sciences - Pediatrics
University of Alberta

## Abstract

The obstruction of blood flow to regions of an infant brain leads to a reduction of oxygen and essential nutrients, causing what is known as hypoxic-ischemic (HI) damage to that region. Presently the only treatment available for affected neonates is hypothermia: head or whole-body cooling. Despite its limited effectiveness, hypothermia delays disease progression, thereby providing an opportunity for a supplement therapy to be beneficial within that time frame. It has long been the goal to combine hypothermia with pharmacology to improve the overall neuroprotective potential. Many drugs have shown promise in treating the HI damaged neonate brain, however, the systemic dosage used to achieve therapeutic concentrations in the brain lead to significant side-effects that have prevented their use in clinic.

Self-assembling peptides can be engineered to respond to biological cues and deliver drugs in an on-demand manner. Although some classical pH sensitive polymer systems have been studied in the past, we focus on using relatively biocompatible elastin-like polypeptides (ELPs) as a self-assembling peptide that can be engineered to respond to pH and temperature to allow for localized release of drug. ELPs are biopolymers composed of repeating units of the pentapeptide sequence Val-Pro-Gly-X-Gly (VPGXG), where the variable residue X can be manipulated to trigger the phase transition at desired conditions. Once in nanoparticle form, appropriate drugs can be incorporated into the ELPs such that hypothermia and/or the pH changes that arise due to disrupted metabolism in the damaged tissue, would induce nanoparticle dissolution. Subsequently, the drug would be released at the site of injury in a safe and controlled manner.

ELPs were synthesized from genetically engineered plasmids in recombinant *Escherichia coli* and purified from the bacterial lysate by inverse temperature cycling (ITC). Dexamethasone (DEX) was selected as the candidate anti-inflammatory drug for neonatal brain injury. Dynamic light scattering was used to characterize the temperature-dependent assembly of ELP nanoparticles containing DEX followed by the pH-dependent disassembly. The drug loading or encapsulation efficiency and the stability of the nanoparticles over time, was determined using high-performance liquid chromatography. Next, the ELP-DEX nanoparticles were injected in a neonatal rat model of brain injury and focal brain cooling was applied. To test the ability of the ELP nanoparticles to deliver DEX to the injured brain, HPLC was used to detect and measure the amount of DEX in the brain tissue.

On screening several valine, leucine, and histidine containing-ELPs in the guest position, we identified the construct (AG)40-(VH4)24 as the one that could undergo nanoparticle formation with DEX encapsulation under physiologically relevant pH 7.4 and temperature 37°C. This construct demonstrated assembly between 35 – 40 $^{o}$C to form particles of size ~300 nm, and disassembly between 35 – 33 $^{o}$C to <10 nm, at 0.25 mg/mL and pH 7.4. When the pH of the solution was lowered to 6.4 during cooling, the disassembly temperature decreased by 1$^{o}$C and at pH 6 complete dissociation was observed, with presence of ~10 nm particles across all temperatures below 45°C. This shows the pH-responsiveness and sensitivity of the ELP construct (AG)40-(VH4)24 within a narrow pH range between 7.4 and 6, is an important trigger owing the local acidosis (~pH < 6.75) that develops at the site of brain injury. The drug loading or encapsulation efficiency of the particles was determined to be 1.3 ± 0.6 % at the same concentration of 0.25 mg/mL.

Selective brain hypothermia was induced using a focal cooling device. Our method of cooling was successful in establishing and maintaining a temperature differential of 3.2ºC between the head and body of the animal throughout the experiment. It also offered the same extent of neuroprotection as in whole-body hypothermia and significantly reduced the amount of tissue damage when compared to normothermic animals ($p$ = 0.0457). A single injection of DEX containing-(AG)40-(VH4)24 particles resulted in ~0.4 µg of DEX/g of brain tissue thus validating the ability of ELP nanoparticles to release DEX in the brain.

The findings suggest that this drug delivery system holds immense potential to enhance the beneficial effect of hypothermia in a clinical setting, thus improving the quality of life in infants with brain injury. The proposed nanoparticles could then be used to understand the effects of multiple drugs under investigation for the treatment of other brain disorders.

## Preface

This thesis is an original work done by Rukhmani Narayanamurthy. All animal experiments were performed in accordance with protocols approved by the University of Alberta Animal Care and Use Committee (AUP00003792_REN1, AUP00000363). A portion of introduction section has been published as a review article titled, "Drug delivery platforms for neonatal brain injury" (Narayanamurthy R, Yang JL, Yager JY, Unsworth LD. Drug delivery platforms for neonatal brain injury. Journal of Controlled Release. 2021 Feb 10;330:765-87). RN and JLJY conducted literature review and wrote the manuscript; JLJY illustrated the figures. JYY and LDU provided feedback and finalized the manuscript.

Other researchers assisted with or performed some of the procedures in this study. Mass spectroscopy was done by Mr. Jack Moore, technician at the Alberta Proteomics and Mass Spectrometry Facility. DNA sequencing was performed at the University of Alberta Molecular Biology Service Unit. Carotid artery ligation surgeries and intraperitoneal injections were done by Mr. Edward Armstrong. HPLC protocols were by developed by Rukhmani with guidance from Mr. Audric Moses, technician at the University of Alberta, Lipidomics Core facility. Optical imaging of the animal organs was done at the Molecular Biology Core Facility in the Alberta Diabetes Institute, University of Alberta. The ELP genes used in this study were cloned by Dr. Jonathan Yang. Rukhmani worked on Western analysis alongside Dr. Yang while quantification and illustration of the protein blots were done by him. Dinuka Waduthanthri optimized the ELP labeling protocol and worked with Rukhmani on obtaining DLS measurement replicates.

All other portions of this thesis are original works.

**Acknowledgements**

I would like to express my heartfelt gratitude to my supervisors Prof. Larry Unsworth and Prof. Jerome Yager. Thank you very much for your patience and exceptional guidance and support, especially during lab shutdowns due to the pandemic. Thank you for giving me the opportunity to learn and grow as well as for the advice that has helped me determine the next steps in my research career. Thank you Dr. Eytan Wine for being on my committee and for your time, advice, and insightful feedback.

A very special thanks to Jonathan and Ed, for your expertise, advice and mentorship, all of which have helped me navigate through some tough times in graduate school. Thank you, Jonathan, for being so patient with me and for offering immense support whenever I needed it even outside of my thesis project. Thank you, Markian, for all your mentorship, help in troubleshooting and contagious energy; your enthusiasm for research is an inspiration to me. Thank you very much Dinuka, for all your help, patience, advice, tips, and tricks and for being a great colleague. Lastly, I would like to thank all the past and present members from both Yager and Unsworth labs: Zeenat, Shammy, Mehdi, Shu Hui, Meng Yi, for your support.

Mikhaila and Trish, thank you for your prompt responses and for getting things done for me. You were amazing! I would also like to thank Audric from the Lipidomics Core facility for his technical assistance.

I am extremely grateful to all my friends, for being there for me whenever I needed them, especially, Sam; Thank you so much for all your time helping me practice presentations, discuss papers and what not! Thank you very much mom and dad for always being my biggest cheerleaders and for encouraging me to carve my own path in life.

This project was funded through the generous support of (i) University of Alberta, Faculty of Medicine and Dentistry, Department of Pediatrics, Maternal and Child Health Scholarship Program, (ii) Alberta Innovates Graduate Student Scholarship Program and (iii) Women and Children's Health Research Institute Graduate Studentship Program (iv) Canadian Institutes of Health Research.

**Table of Contents**

**List of Tables**

**List of Figures**

**List of Abbreviations**

| | |
|---|---|
| Act b | β-actin |
| AMPA | α-amino-3-hydroxy-5-methyl-4-isoxazolepropionic acid |
| ATP | Adenosine triphosphate |
| BBB | Blood-brain barrier |
| BCA | Bicinchoninic acid |
| Casp3 | Cysteine-aspartic acid protease 3 |
| cc | Corpus callosum |
| COX | Cyclooxygenase |
| CMT | Critical micelle temperature |
| ctx | Cortex |
| CXCR4 | C-X-C chemokine receptor type 4 |
| Cy5 | Cyanine 5 |
| DEX | Dexamethasone |
| DG | Dentate gyrus |
| DNA | Deoxyribonucleic acid |
| DLS | Dynamic light scattering |
| ELP | Elastin-like polypeptide |
| EPO | Erythropoietin |
| Gfap | Glial fibrillary acidic protein |
| H&E | Hematoxylin and eosin |
| HI | Hypoxic-ischemic/hypoxic-ischemia |

| | |
|---|---|
| HPLC | High performance liquid chromatography |
| hy | Hypothalamus |
| Iba1 | Ionized calcium-binding adapter molecule 1 |
| IL | Interleukin |
| iNOS | Inducible nitric oxide synthase |
| IPTG | Isopropyl β-D-1-thiogalactopyranoside |
| ITC | Inverse temperature cycling |
| iTEP | Immune tolerant elastin-like polypeptide |
| LOD | Limit of detection |
| lv | Lateral ventricle |
| NADPH | Reduced nicotinamide adenine dinucleotide phosphate |
| NHS | N-hydroxysuccinamide |
| NMDA | N-methyl-D-aspartate |
| NO | Nitric oxide |
| PD | Postnatal day |
| PBS | Phosphate buffered saline |
| PEG | Polyethylene glycol |
| PLGA | Poly(DL-lactic-*co*-glycolic acid) |
| PDC | Pyruvate dehydrogenase complex |
| RDL | Recursive directional ligation |
| ROS | Reactive oxygen species |
| RNOS | Reactive nitrogen and oxygen species |

| | |
|---|---|
| SDF-1 | Stromal cell-derived factor 1 |
| SEM | Standard error of mean |
| $T_t$ | Transition temperature |
| th | Thalamus |
| TNF-α | Tumor necrosis factor-α |
| TPER | Tissue protein extraction reagent |
| VEGF | Vascular endothelial growth factor |
| 3v | Third ventricle |

# Chapter 1: Introduction

**Portions of this chapter have been published in:**

Narayanamurthy R, Yang JL, Yager JY, Unsworth LD. Drug delivery platforms for neonatal brain injury. Journal of Controlled Release. 2021 Feb 10;330:765-87.

### 1.1 Neonatal hypoxic-ischemic brain damage

Hypoxic-ischemic (HI) brain damage, resulting from the interruption of oxygen and blood supply to the neonate brain around the time of birth, is a risk factor for mortality and several lifelong neurological impairments **[1,2]**. In babies that survive the damage, it may manifest as epilepsy, cerebral palsy, motor and cognitive decline, attention-deficit hyperactivity disorder, and behavioral disabilities **[1-3]**. Chronic maternal eclampsia, umbilical cord knotting or collapse, shoulder dystocia and placental abruption are some of the possible factors that can cause HI injury **[1]**. Some of the long-term outcomes develop in at least 25% of the infants, even if they have mild HI injury **[4-7].** As one of the prime causes of infant mortality and chronic morbidity worldwide, its incidence has been reported to be up to 6-8 births per 1000 live births in developed countries with roughly 26 per 1000 live births in developing countries **[8-10]**.

HI injury is commonly characterized with two zones, namely, the core and the penumbra **[11,13]**. In the core, necrotic cell death occurs rapidly since this is where oxygen deprivation, ischemia, and complete energy depletion is most severe **[11]**. It acts as the focal point for the evolution of the ischemic cascade. The penumbra is region surrounding the core, where both ischemia and anoxia are incomplete. Studies have detailed that the core is comprised of both necrotic and apoptotic cells, whereas the penumbra predominantly contains apoptotic cells **[12,13]**. If the penumbra could be targeted to promote cellular survival it is possible that the entire region could be rescued, and functional recovery restored after an HI injury **[14]**.

### 1.1.1 Pathophysiology of neonatal HI brain injury

HI insult triggers an ischemic cascade that is dynamic and can persist several days or weeks **[15]**. Low levels of oxygen in the brain depletes high energy phosphate reserves within minutes post HI, causing inactivation of the Na-K ATPase pump **[16,17]**. This leads to an influx of sodium and water with efflux of potassium, thereby resulting in cell edema. The excess intracellular sodium leads to uncontrolled neuronal depolarization and release of excitatory neurotransmitters **[18,19]** and further perpetuates the injury. However, some neurons can partially recover from HI incidence in the latent phase due to transient mitochondrial function and restoration of cerebral circulation, thus providing a window of opportunity for interventions to ameliorate the impact of subsequent secondary energy failure **[17,20]** characterized by impaired oxidative metabolism, secondary edema, seizures, and apoptotic neuronal death **[20,21].** The tertiary phase can last for months or years after the initial insult, with continued activation of inflammatory responses, reduced plasticity due to impaired synaptogenesis, damage to oligodendrocytes and epigenetic changes **[22]**. All the different phases of HI injury thus involve the complex interplay of free radicals, pro-inflammatory cytokines, and excessive glutamate **(**Figure 1**) [22]**.

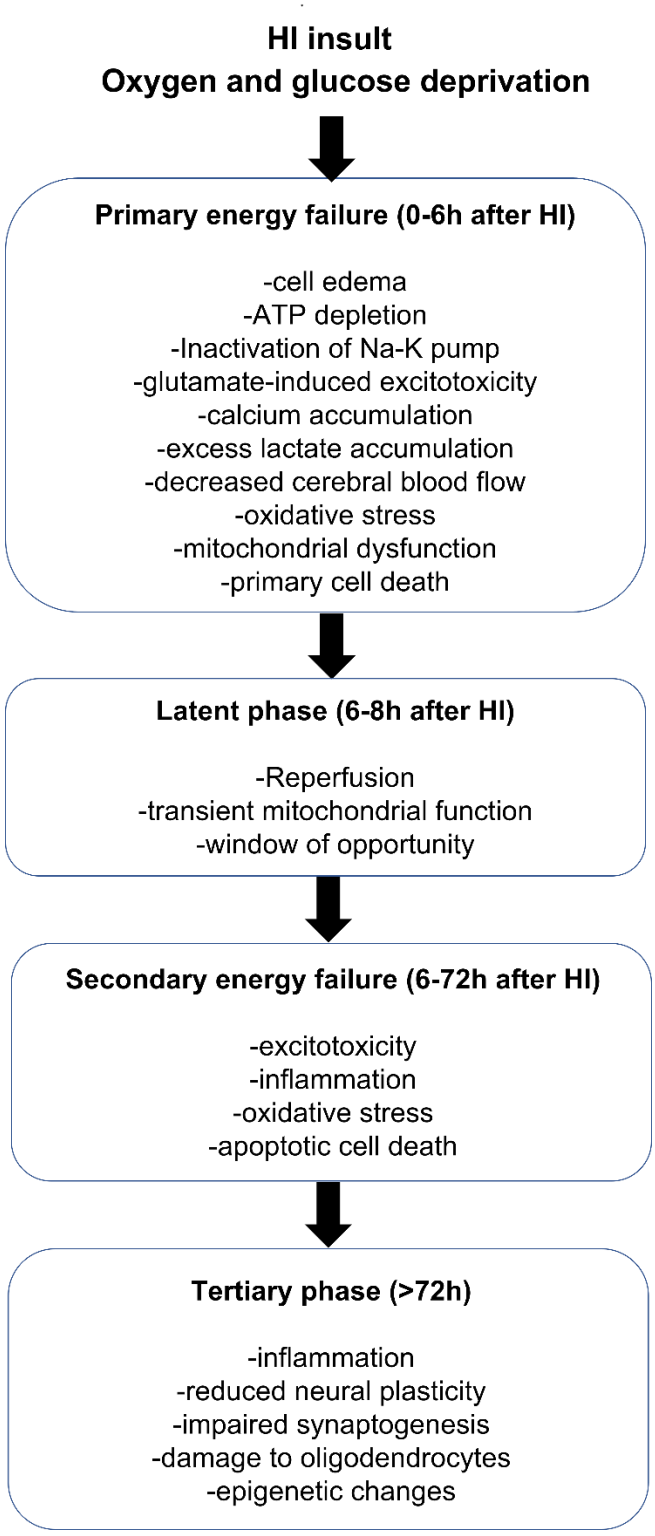


**Figure 1.** A flowchart depicting the different phases in the pathophysiology of HI injury.

#### 1.1.1.1 Oxidative stress

The newborn brain is highly susceptible to oxidative stress due to decreased expression of endogenous antioxidant enzymes such as superoxide dismutase and glutathione peroxidase **[23]**. In addition, it has high amounts of unsaturated fatty acids prone to peroxidation by the reactive oxygen and nitrogen species (RNOS) which get accumulated in high concentrations due to impaired metabolism **[24,25]**. The oxidative modification of lipids, proteins and DNA by the free radicals eventually leads to mitochondrial dysfunction and cell death. The enzymes involved in the mitochondrial electron transport chain, NADPH oxidases, xanthine oxidase, arachidonic acid, and nitric oxide (NO) synthase are responsible for the generation of these free radicals **[26]**. NO synthase facilitates progression of the ischemic cascade by production of NO free radicals which can in turn increase expression of apoptotic proteins and proapoptotic genes **[25,26]**.

Free radicals can also contribute to disruption of brain tissue homeostasis, causing local tissue acidosis at the site of damage post HI injury **[26, 27]**. Excessive buildup of reactive oxygen species (ROS) will impede the function of the pyruvate dehydrogenase complex (PDHC) in the inner mitochondrial membrane. This combined with a reduction in the ability to transfer reducing power from glycolysis generated NADH to the mitochondria would cause lactate dehydrogenase, which is activated by increased calcium ion concentration, to utilize NADH to produce huge quantities of lactate. Consequently, acidosis results from the excessive lactate buildup in the cytosol of neurons **[27]**. Data from clinical studies also demonstrate an increase in cerebral lactate concentrations and decrease in pH in infant brains within 0-6h of HI incidence **[27].**

Calcium ions play an important role in signal transduction as a secondary messenger and hence their intracellular concentration is usually maintained at low levels by several mechanisms involving ion pumps, transporters, and channels **[28,29]**. However, after the onset of hypoxia, the intracellular calcium levels increase in response to stimulation of the NMDA receptor channels by glutamate **[27]**. Increase in intracellular concentration of calcium is harmful since it can cause the activation of various calcium-dependent ATPase enzymes, lipases, deoxyribonucleases and proteases which can mediate irretrievable death of developing neurons **[30]**. It can also act *via* a calcium/calmodulin dependent mechanism and trigger the synthesis of NO free radicals by the activation of NO synthase **[26]**. Besides intracellular increase in calcium levels, elevated calcium concentrations within the mitochondria can lead to loss of nicotinamide adenine dinucleotide, which is crucial for ROS detoxification and maintenance of cellular metabolism **[27]**.

#### 1.1.1.2 Excitotoxicity

As mentioned previously, disruption of cellular homeostasis follows HI due to reduction in ATP levels and inability of the cell to maintain ionic gradients **[31]**. This in turn causes excessive release of glutamate into the synaptic cleft leading to prolonged stimulation of neurons and other cells that express extracellular excitatory amino acid receptors such as AMPA, NMDA and kainite receptors **[32]**. The consequent increase in calcium influx, in turn leads to increased free radical production, caspase activation, mitochondrial dysfunction and other mechanisms that ultimately lead to apoptosis **[33, 34]**. Additionally, prolonged HI leads to failure of re-uptake of the extra-synaptic glutamate by glial cells, thus preventing normal synaptic transmission, further promoting excitotoxicity **[34, 35]**.

#### 1.1.1.3 Inflammation

Innate immune response acts as the first line of defense in response to HI injury in the developing brain. At the outset, the microglia are activated and attain macrophage-like functionalities such as phagocytosis, antigen presentation, production and release of matrix metalloproteinases and cytokines **[36,37]**. Microglial activation can lead to disruption of blood brain barrier which facilitates the entry of other neurotoxic substances and peripheral leukocytes into the cerebral parenchyma and worsen the damage **[36]**. Besides microglia, overactive astrocytes also contribute to the evolution of damage by production and release of pro-inflammatory cytokines (IL-6, TNF-α, IL-1α, and β and interferon γ) and chemokines, which chemokines determine the level of immune cell accumulation at the site of injury **[38-40]**. Cytokines such as IL-1 and IL-6 serve as sources of reactive oxygen species (ROS) while IL-1β can lead to development of seizures **[41,42]**. Moreover, under conditions of pro-inflammatory stimuli, nuclear factor-κB (NF- κB) is activated and targets downstream inducible genes that produce iNOS, COX-2 and cytokines, which are involved in inflammatory response and apoptotic cell death following cerebral ischemia **[13]**.

#### 1.1.1.4 Mitochondrial dysfunction

Mitochondria has a central role to play in the progressive nature of HI injury by regulating the apoptotic pathways, thus determining the fate of cells. As an intracellular calcium buffer, its dysfunction can lead to increased intracellular calcium concentrations, leading to a chain of events associated with cell death **[26,35]**. In addition, the process of ATP generation by the electron transport chain is interrupted due to excessive production and accumulation of ROS within the mitochondria. Without enough energy to maintain the ionic gradient across the membrane, inflow

of calcium ions increases, thus forming a vicious cycle **[27]**. Furthermore, mitochondrial membrane permeability is disrupted due to the oxidation of proteins and lipids in the inner mitochondrial membrane, subsequently activating the mitochondrial permeability transition pore *via* activation of pro-apoptotic proteins **[43]**. This in turn causes leakage of cytochrome c into the cytoplasm which would interact with the apoptotic protease activating factor, thus forming the apoptosome which activates a series of caspases (pro-caspase-9, caspase-9 and 3) that cause DNA fragmentation and programmed cell death **[44]**. Although cell death predominantly occurs by apoptosis other forms of cell death such as autophagy and necrosis can occur during neurodegeneration in neonatal HI **[26]**.

### 1.1.2 Blood brain barrier in neonatal HI brain injury

HI injury alters the blood-brain barrier (BBB). The differential gene expression of BBB components comprising of tight junction proteins, extra-cellular matrix constituents and adhesion molecules, plays a key role in determining its integrity post HI insult in the neonatal brain **[44, 45]**. The fragility of the newly formed blood vessels, coupled with support from a smaller number of astrocyte end feet compared to a fully developed brain, increases the vulnerability of the BBB in the immature brain to HI damage **[2]**. Several studies have demonstrated the increase in the endothelial permeability of the BBB due to the stress-induced signals (pro-inflammatory mediators and free radicals) produced in the HI brain, both in animal and human neonates **[46-48].** While recovery of the BBB has been observed in adult animal models, the neonate condition remains ill-defined **[49]**. The fact that the BBB is disrupted at the injury site could therefore be harnessed to introduce therapeutic agents into the neonatal brain for treating HI induced brain damage.

### 1.1.3 Therapeutic hypothermia as the standard of care

Therapeutic hypothermia is regarded as the global standard of care for neonatal HI brain injury **[50-52]** and is currently the only licensed treatment for moderate to severe HI injury **[2,53,54]**. Numerous randomized controlled trials have demonstrated the capability of hypothermia in terms of improved survival rates and reduced risk of neurodevelopmental disorders such as cerebral palsy **[54]**. Although the exact mechanisms are ambiguous, studies using rodent models of neonatal HI brain damage have shown that the neuroprotective mechanism of hypothermia is primarily attributed to immunosuppression *via* inhibition of microglial activation and the reduced cellular metabolic rate at lower temperatures **[15,55]**, thus decreasing the demand for oxygen and ATP to sustain tissue viability. It has also been shown that it interferes with the excito-oxidative cascade by reducing free radical formation, accumulation of excitatory amino acids. **[56,57]** and prevent lipid peroxidation of cell membranes **[52,59]**.

There are multiple methods used to induce cooling in both patients and animal models. It can be administered as either head cooling or full body cooling **[52,58]** and is most effective when initiated within 6h of birth in infants within the incidence of HI **[52, 54]**. The depth of hypothermia is stratified clinically as 31°C (moderate) to 36°C (ultra-mild) **[60]**, where current guidelines prescribe cooling to 33.5°C for 72 hours in term neonates with hypoxic-ischemic brain injury.

Despite many drug therapies that have shown promising results in in vitro and animal models of HI brain injury, hypothermia is the only treatment that has been successfully translated for application in neonates **[58].** However, it only offers partial protection, is not curative and high

mortality and neurological complications persist even in infants subjected to hypothermia **[50,53,54].** In addition, a paucity of information regarding long-term outcomes post HI injury and minimal feasibility in low-income countries remain as some of its setbacks **[56]**. Nevertheless, even in studies where it has shown limited effectiveness, hypothermia has shown to extend the therapeutic window for treating HI damage, thus providing an opportunity to employ secondary therapies (i.e., drugs) during this time to help rescue the tissue from further damage **[61,62]**.

### 1.1.4 Therapeutic agents in neonatal brain injury

In response to injury, the brain may upregulate the expression of endogenous trophic factors to attenuate the spread of damage and promote regeneration. However, relying on endogenous mechanisms of neuroprotection and repair is insufficient for recovery. Therefore, the objective has been to supplement the damaged brain with critical factors to further drive the recovery process. The pathophysiology of stroke in adults and neonatal brain injury, both have overlapping presentations of excitotoxicity, inflammation, neurodegeneration **[49, 63]**. Thus, the therapeutic strategies, explored initially in adult rodent models of stroke, are now investigated for treating neonatal hypoxic-ischemic brain damage. Similarly, targeting the biochemical cascades associated different phases of injury progression with pharmacological agents, has been an active approach adopted by several preclinical and clinical experiments. This is being explored either in a standalone manner or in combination with hypothermia since it is the established treatment of care for neonatal HI brain injury **[63]**.

### 1.1.4.1 Growth factors

Growth factors are among the most promising candidates for treating neonatal HI brain injury. However, clinical application of growth factors has been impeded by poor BBB permeability, high dosages required to achieve neuroprotection, limited therapeutic half-life, and side-effects of systemic administration such as bone pain and increased hematocrit **[63, 64]**. A solution may come from targeted delivery of therapeutics to the injured site of the brain for reducing the systemic dose while locally maximizing the beneficial effects.

Among the growth factors, erythropoietin (EPO) has shown substantial potential as a neuroprotective agent, especially in animal models through its anti-inflammatory, antioxidant, anti-excitotoxic, anti-apoptotic, neuroregenerative, and angiogenic properties **[63,65,66]**. It has also been studied as a combination treatment with hypothermia **[67]**. Although, it conferred neuroprotection against HI brain injury **[68]** in neonatal studies, intravenous administration of EPO to adult stroke patients produced unfavourable effects, including patient death, attributable to the high dose of EPO over a brief time of 6-48 h **[69]**. Nevertheless, it is a promising candidate, closest to clinical translation for the treatment of neonatal HI brain injury, with further research required regarding its dosage and time of administration.

### 1.1.4.2 Small molecules

Melatonin, magnesium sulfate, topiramate, phenobarbital, cannabidiol and allopurinol alongside noble gases such as xenon and argon, are other small molecules that have been studied extensively for their neuroprotective properties. Out of these melatonin, Xenon gas and phenobarbital have been widely tested as an adjunct to hypothermia **[63]**.

#### 1.1.4.3 Glutamate channel blockers

Early treatments of HI brain injury centred on inhibiting the initial phases of injury, i.e., excitotoxicity and oxidative stress **[70]**. However, many of the agents failed because it is not possible to block essential physiological processes, such as glutamatergic transmission, without causing additional damage. As such, several NMDA receptor antagonists increased, rather than decreased, cell death **[71]**. An exception is magnesium sulfate. Treatment with magnesium sulfate has reduced the incidences of moderate to severe cerebral palsy **[72]**. Magnesium alleviates excitotoxicity by decreasing calcium or glutamate signalling **[73]** and has anti-inflammatory and antioxidant effects **[74]**.

#### 1.1.4.4 Combination treatments

Administering xenon in combination with hypothermia ameliorates structural and functional outcomes in neonates, and the benefits are maintained through adulthood **[75]**. Similarly, phenobarbital, an anti-convulsant, when administered with whole-body hypothermia, was found to curb neurodevelopmental outcomes, and reduce mortality and the frequency of seizures **[76]**. Melatonin was shown to exert neuroprotective effects in rodent models, more prominently when used with whole-body hypothermia, by reducing oxidative stress, inflammation, apoptosis, and mitochondrial dysfunction **[77]**. This was also proven to be beneficial in term and preterm infants **[77]**. Despite demonstrating favourable outcomes, more investigation is required to translate these molecules into clinical practice through extensive research on their dose-response relationship, optimal time, and route of administration.

## 1.2 Dexamethasone as a neuroprotective agent

As previously described in Section 1.1.1.3, one of the critical mechanisms that mediates hypoxic-ischemic brain injury is neuroinflammation, characterized by microglial activation and infiltration of glial cells, monocytes, and T-cells. The secretion of pro-mediators like cytokines, chemokines, ROS, and excitatory neurotransmitters by the active immune cells mount an inflammatory response that exacerbates damage to the brain by causing demyelination, scarring, further disruption of the BBB, and apoptosis of neurons and oligodendrocyte precursors **[2,63]**. Despite being one of the early responders to injury, immune system activation may require several hours to fully develop after the incidence of HI **[78]**. Intervention with anti-inflammatory drugs during this period might suppress or prevent the upregulation of inflammatory pathways involved in the injury cascade.

Dexamethasone (DEX) is a synthetic glucocorticoid and glucocorticoid receptor agonist **[78].** It is being studied extensively in the treatment of neonatal HI brain injury owing to its anti-inflammatory properties and neuroprotective effects **[78-80]**. Several *in vivo* experiments in neonatal rodent models of HI brain injury demonstrate the therapeutic potential of DEX by reducing the exacerbation of brain damage *via* various mechanisms. For instance, subcutaneous injection of 0.5 mg/kg DEX given 5 hours prior to HI damage in PD7 rats, elicited neuroprotection by reducing the number of CXCR4 receptors and binding efficiency of SDF-1 alpha **[79]**. Similarly, two-dose intraperitoneal administration of 0.25 mg/kg/dose of DEX, 24h and 4h prior to HI insult, increased the gene and protein expression VEGF and Akt phosphorylation and reduced capsase-3 activity, in PD7 rats **[81]**. In a long-term behavioral study, a singular dose of intraperitoneal DEX injection at 0.5 mg/kg, offered protection against extensive damage to the

striatum and the hippocampus, which was mirrored in improved memory functions and decreased attention deficits in treated vs untreated groups **[82]**.

Despite convincing evidence in pre-clinical studies as a potent molecule for the treatment of inflammation in HI brain injury, clinical trials in adult stroke patients suggest otherwise **[83]**. DEX can also have toxic side effects in infants when administered systemically **[84]**; thus, it is necessary to administer the drug precisely to the injured brain tissue and minimize its concentration in circulation.

### 1.3 Elastin-like polypeptides

Self-assembling peptides can be engineered to respond to biological cues and hence can be used to deliver drugs in an on-demand manner **[85,86]**. Elastin-like polypeptides (ELPs) are peptides that exhibit an interesting property: they can be programmed at the amino acid level to assemble and disassemble in response to environmental stimuli, such as pH, temperature, ionic strength, electrical current, redox agents, and light **[87-89]**. Of these factors, the temperature-dependent response is the best characterized. ELPs consist of repeating units of the pentapeptide motif Val-Pro-Gly-X-Gly (VPGXG), where the variable or guest residue X can be manipulated to trigger the phase transition at desired conditions **[88]**. The guest residue can be any amino acid besides proline since an additional proline with its imidazole ring can produce stearic hindrance and interfere with the reversible phase transition of the ELP **[90]**. Once in nanoparticle form, appropriate drugs can be incorporated into the ELPs such that hypothermia or the pH changes that arise due to disrupted

metabolism in the damaged tissue **[27]**, would induce nanoparticle dissolution **[86-88]**. Subsequently, the drug would be released at the site of injury in a safe and controlled manner.

### 1.3.1 Temperature-dependent phase transition behavior

ELP diblock co-polymers are amphiphilic in nature, containing hydrophilic and hydrophobic domains that differ in the guest amino acid composition within the pentapeptide sequence **[91]**. A particular temperature above which the ELPs undergo conformational change due to decreased solubility is termed as Transition temperature or Tt **[88]**. Besides external factors, $T_t$ is influenced by the intrinsic properties of the ELP, such as the ELP guest amino acid, its molecular weight, chain length, and concentration in solution **[92]**. ELPs that are composed of longer chains or hydrophobic guest amino acids are expected to exhibit a lower $T_t$ compared to their counterparts with hydrophilic residues and shorter sequences **[89,93]**. Although the factors that determine the Tt and their effects have been well-documented, the exact mechanisms by which the ELP demonstrate reversible phase transition remain poorly understood **[88]**. The self-assembly process of diblock ELPs is thought to be prompted by the ratio of hydrophobic to hydrophilic groups that constitute the molecule **[94]**. At lower temperatures, ELPs are miscible in water. However, when the temperature is increased beyond a threshold, the water molecules bound to the hydrophobic groups are released, thus decreasing the Gibbs free energy of the system making the process thermodynamically favourable **[95-97]**. The resultant entropic gain drives the self-association of the hydrophobic groups to result in micro-to-nanoscale micellar structures with a hydrophobic core and a hydrophilic exterior **[98-100]**.

### 1.3.2 pH-responsive behavior

The distinct pH responsive nature of ELPs is conferred by the presence of histidine residues in the diblock **[85-87]**. If pKa of a compound is greater than the pH of its surrounding, then it gets protonated due to the increased hydrogen ion concentration in the medium. Therefore, at pH 7.4, predominant number of histidine residues will remain uncharged since histidine's side chains have a lower pKa of 6 **[85-87]**. The relative increase in the hydrophobicity of the histidine-rich segment due to the uncharged residues, will consequently drive the assembly of micellar structures above a certain temperature **[85-87]**. On the other hand, a decrease in pH will increase the hydrophilicity of the histidine residues owing to their protonation, thus weakening the strength of the non-covalent interactions that enable nanoparticle formation, resulting in disassembly **[85-87]**.

### 1.3.3 Biomedical applications

ELPs are synthesized from DNA templates in genetically engineered *Escherichia coli*. The highly repetitive sequences and GC-rich domains in the genes encoding for ELPs create challenges in genetic manipulation **[101]**. Thus, conventional genetic techniques, such as polymerase chain reaction, are impractical for ELP gene construction. Instead, nucleotides encoding a fragment of the ELP repeating unit can be synthesized chemically and concatemerized by recursive directional ligation (RDL) to obtain the desired ELP length **[102]**. RDL involves the application of Type II restriction enzymes to generate DNA fragments with distinct 5'- and 3'-termini that can be spliced together to elongate the ELP gene while preserving the biochemical orientation and finally inserted into a plasmid vector for gene amplification or expression in *E. coli* **[101,102]**. ELPs can be isolated from transgenic *E. coli* by inverse temperature cycling (ITC); through rounds of heating

and cooling, the ELP is sequentially isolated from the impurities by phase separation **[101,102]**. Unlike traditional chemical methods of polymerization, the genetic approach to ELP synthesis allows unique and precise control over ELP length and sequence and monodispersity **[103]**. This in turn offers control over the tunable physicochemical properties of the ELPs such as their characteristic self-assembling and stimulus-responsive nature, making them desirable for a variety of biological applications such as protein purification, tissue engineering, and controlled drug release. There are multiple reviews that discuss the different ways that ELPs are developed for specific purposes **[90,92,103,104].**

Tissue engineering is one amongst the fields where ELP can be applied owing to its highly customizable scaffold thereby making it befit for *in vivo* applications. The temperature sensitivity of the ELPs can be utilized to formulate them into injectables to facilitate healing of the injured tissue by providing a suitable biochemical and physical environment that stimulates cell growth and differentiation **[105]**. Articular cartilage damage is one the areas where ELPs have been widely used. This tissue has limited regenerative ability and one of the promising methods for treating damage to this tissue is by transplanting chondrocytes into ELP-based scaffolds. ELP scaffolds have shown to promote chondrocyte differentiation and support the synthesis of extracellular matrix for articular cartilage repair **[106]**.

The preservation of the reversible phase transition property of ELPs in ELP fusion proteins, allows them to be utilised as a tag to purify other proteins by means of ITC. ITC can be used to purify ELP fusions, and the ELP can be removed using a proteolytic cleavage site or a self-excision intein

(a self-splicing protein domain) placed between the ELP and the target protein **[103]**. A study by Carlson et al (2004) where they compared the efficiency of ITC with immobilised metal affinity chromatography for protein purification, showed that ITC is more advantageous since it can be scaled to produce high-yield proteins using readily accessible labware and instruments **[107,108]**. In reviews by Hassouneh et al (2010) and Yeboah et al (2016), the employment of ELPs as a purification tag for efficient separation of proteins has been discussed more in depth **[109,110]**.

In terms of drug delivery systems, ELPs are engineered to self-assemble or aggregate into different forms of drug carriers such as nanoparticles or block copolymers with varying architectures **[92]**. Besides their attractive physicochemical properties, their non-toxic degradation products, low immunogenicity, and biocompatibility make them suitable for *in vivo* use **[111]**. Packaging drugs inside ELPs can improve their pharmacokinetics by increasing the plasma half-life and drug bioavailability due to the high-molecular weight of the ELPs which place them above threshold for renal clearance **[112, 113]**. This also increases their circulation time in blood by retention for longer durations.

With cancer treatment ranking the most prevalent sector where ELPs are under tremendous development, research on ELP as nanomedicine has also pioneered in the fields of ophthalmology, gene delivery and maternal-fetal medicine. Massodi et al were one of the first groups to design a 120-mer ELP with a 1:7:8 ratio of valine, glycine, and alanine at the guest amino acid position fused with a range of cell penetrating peptides that entered cervical and ovarian cancer cells **[114]**. These hybrid constructs reduced cell proliferation when combined with a kinase inhibitor.

Similarly, ELP hydrogel scaffolds that can be loaded with appropriate antibiotics for their sustained release to treat local infections have been developed **[115,116]**. As a vaccine carrier, Cho et al generated an immune tolerant ELP (iTEP) nanoparticle composed of a diblock copolymer of iTEP and cytotoxic T lymphocyte peptide vaccine. When injected into mice, these nanoparticles enhanced the presentation of the vaccine by dendritic cells and increased strength of the vaccine-induced cytotoxic T lymphocyte response **[117]**. A more elaborate discussion on drug delivery systems based on ELPs and their applications have been presented in several review paper **[92, 104, 118,119].**

## 1.4 Hypothesis

The developed ELP nanoparticles will release encapsulated drug (dexamethasone) in response to temperature and pH, at the site of injury.

## 1.5 Objectives

i) Express and purify diblock ELP constructs.

ii) Characterize the thermal and pH responsive behavior of the constructs in the presence of dexamethasone.

iii) Screen the ELPs to determine the construct that can assemble and disassemble within the temperature and pH range of interest i.e., 31 to 40°C and 6.4 to 7.4.

iv) Determine the *in vivo* biocompatibility of ELPs.

v) Assess the drug release efficacy of the ELP nanoparticle system loaded with dexamethasone in seven-day old Long Evans rats with HI brain injury under hypothermic and normothermic conditions.

# Chapter 2:

# Methodology

## 2.1 Animal care and use

For animal studies, seven-day old Long-Evans rats were used since its developing brain is equivalent to that of a human baby born either term or pre-term with approximately 36-40 weeks of gestation **[120]**. The Rice-Vannucci model of HI brain injury in the neonatal rat is the model under consideration.

Adult Long-Evans rats were obtained from Charles River Laboratories (Montreal, Canada) and were kept on a 12-hour light-dark cycle with free access to food and water. Pups were bred in-house and delivered vaginally, with the day of birth recorded as postnatal day 1 (PD1). PD7 male and female rat pups weighing between 12-16 g were used for experiments. All experimental procedures were carried out in agreement with the guidelines issued by the Canadian Council on Animal Care and were approved by the Animal Care and Use Committee at the University of Alberta (AUP00003792_REN1, AUP00000363).

## 2.2 Induction of HI injury

The PD7 rat pups were anesthetized using isoflurane (4% induction and 2% maintenance in 30% $O_2$ and 70% $N_2O$) prior to surgery. A longitudinal incision was made in the neck to expose the right common carotid artery, and the artery was permanently ligated using a 5-0 silk surgical suture. The incision was sutured closed. The animals were then allowed to recover from anesthesia for 2 hours with their dams. To induce hypoxia, the animals were exposed to a mixture of 8% oxygen-92% nitrogen for 90 min. inside 500 mL glass jars submerged in a water bath at 37°C.

### 2.3 ELP gene concatemerization and cloning

ELPs were obtained according to established protocols **[101]** with minor modifications. The ELP expression vectors were obtained by a process known as recursive directional ligation where a series of identical linearized vector DNA are sequentially ligated to produce ELP genes containing the desired number of repeats. DNA sequences coding for ELPs (Table 1) were custom ordered from Integrated DNA Technologies (Coralville, USA) as inserts in IDT plasmid constructs. The coding DNA sequences were released from the IDT vector by conventional restriction digest with *Eco*RI and *Hin*dIII (all restriction enzymes were purchased from New England Biolabs, Ipswich, USA), ligated using T4 DNA ligase (New England Biolabs) into the pUC19 vector (Bio Basic, Ontario, Canada), and propagated in XL10 Gold chemically competent *Escherichia coli* (Agilent Technologies, Santa Clara, USA). To obtain the desired length and composition of ELPs, the coding DNA sequences were concatemerized by digestion with a combination of *EcoR*I-*Bgl*I and *Eco*RI-*Pfl*MI and ligation of the DNA fragments. The completed ELP DNA sequences were released from pUC19 using *Pfl*MI-*Bgl*I, ligated into the pET-25b(+) vector (EMD Millipore, Ontario, Canada) linearized with *Sfi*I, and transformed into OneTouch BL21 (DE3) *E. coli* (Invitrogen, Carlsbad, USA). Plasmid DNA sequencing was performed at the University of Alberta Molecular Biology Service Unit.

### 2.4 ELP expression and purification

The transformed OneTouch BL21 (DE3) *E. coli* cells were cultured in 1L Terrific broth (Fisher Scientific, Waltham, USA) supplemented with 100µg/L ampicillin and 4ml/L of 100% glycerol in a shaker maintained at 37°C until an optical density of 0.6-0.8 was reached. Expression was induced by the addition of 2mM isopropyl β-D-1-thiogalactopyranoside (IPTG) (Fisher Scientific)

for a period of 24h. The cells were harvested by centrifugation and the cell pellet resuspended in 40 mL phosphate buffered saline (PBS), was stored at -80°C until the purification process. Purification was carried out by inverse temperature cycling (ITC), where ELP is extracted from the crude sample by utilizing its reversible phase transition property **[88,101]**. Cells were lysed by sonication using the Fisherbrand Model 505 Sonic Dismembrator (Fisher Scientific). Polyethyleneimine (0.7%) was added to the lysate and centrifuged to precipitate bacterial DNA. The supernatant was incubated at 60°C for 10 min, set on ice for 10 min, and centrifuged to eliminate impurities from the lysate that irreversibly precipitated by heating. Then, aggregation of the ELP in the supernatant was triggered by the addition of salt (sodium chloride) (Fisher Scientific) and incubation at 37°C for 10 min and the sample was centrifuged at 40°C and 14000g (hot spin) to recover the ELP pellet. The ELP pellet was resolubilized in 2 mL of cold PBS, incubated on ice for 10 min, and centrifuged at 4°C and 14000g (cold spin) to eliminate residual solids. The same cycle of heating and cooling was repeated up to 3 or 5 times to further remove impurities from the bacterial lysate and isolate the ELP.

The final sample of ELP was analyzed by polyacrylamide gel electrophoresis on a 12% separating gel and stained in 0.3 M copper (II) chloride solution (Fisher Scientific) to visually inspect for impurities and to verify the molecular weight. The concentrations of ELPs were quantified using UV absorbance at 280 nm **[88,101]**. The molecular weights of the ELP constructs were confirmed by mass spectroscopy at the Alberta Proteomics and Mass Spectrometry Facility.

## 2.5 Dynamic light scattering experiments

The phase transition behavior of the ELPs was studied in the presence of DEX (TSI America, USA) using dynamic light scattering (DLS) (Malvern Zetasizer Nano ZS, Malvern Instruments Ltd, Malvern UK), between the temperature range of 15°C and 4°5C at 5°C intervals and pH 7.4. The ELP- DEX solution for each construct, was prepared on ice by diluting the ELP using PBS saturated with DEX to attain the desired ELP concentrations of 0.25 mg/mL and 0.5 mg/mL. The samples were then sonicated in an ice bath for 30 mins following which each sample was placed in a DLS cuvette and kept on ice until measurement. Once placed inside the instrument, the samples were heated and subsequently cooled at the abovesaid temperature range with size measured at every 5°C interval. An equilibration of time of 2 mins between every measurement temperature was programmed to enable thermal equilibration of the samples. For every temperature during the heating and cooling cycle, two measurements, each with approximately 15 sub runs were recorded.

## 2.6 Determination of encapsulation efficiency and nanoparticle stability

The encapsulation efficiency of the ELP nanoparticle for (AG)40-(VH4)24 was quantified by determining the amount of free drug present in the aqueous solution using high pressure liquid chromatography (HPLC) (Agilent 1100 series), on separating the loaded nanoparticles from the unbound drug *via* centrifugation. The ELP – DEX solution was prepared using DEX saturated in PBS such that the concentration of ELP in the final solution was 0.25 mg/mL, the concentration at which it formed stable nanoparticles in the presence of DEX at 37°C. The sample was prepared at 4°C and incubated for 10 mins on ice following which it was subjected to a temperature ramp from 15°C to 45°C in 5°C increments using a heat block. It was then centrifuged at 40°C and the

supernatant was run on HPLC to determine the amount of free drug present in the solution. The encapsulation efficiency was then calculated using the following equation:

$$\text{Encapsulation efficiency} = \frac{\text{Total drug } (\mu\text{g}) - \text{Free drug } (\mu\text{g})}{\text{Total drug } (\mu\text{g})} \times 100\%$$

The basic method for determining the amount of free DEX in the sample was based on Grippa et al **[121]**, with reversed-phase HPLC using C-18 column (4.6 x 250 mm; 5µm particle size; 80Å pore size) (Agilent, CA, USA). Flow rate of the mobile phase was set at 1 ml/min. Here, isocratic elution using water and acetonitrile (Sigma-Aldrich Canada Co., ON, Canada) (50:50 v/v) containing 0.1% trifluoroacetic acid (Sigma-Aldrich) was employed and the eluate containing DEX was monitored at 241 nm.

To deduce stability of the nanoparticles at pH 7.4 and 37°C, the samples were prepared in the same manner as mentioned previously, and incubated at 37°C, 180 rpm. Samples were withdrawn on days 0-3 and the encapsulation efficiency was calculated to determine if the amount of drug encased within the nanoparticles, changes over time. This would serve as an indirect measure of nanoparticle stability.

## 2.7 Administration of Selective brain hypothermia using a cooling device

### 2.7.1 Cooling device construction

To localize the effect of hypothermia and selectively cool the head of the rat pup, we designed a cooling device. The cooling device consisted of a temperature-controlled water bath, peristaltic

pump, and cooling units that each accommodate a single rat. The number of cooling units could be scaled to match the number of rats. The schematic of a single cooling unit is presented in Figure 2A. In each cooling unit, the rat head was surrounded by a coil of soft Tygon polyvinyl chloride tubing (inner diameter 1.59 mm, outer diameter 4.76 mm; McMaster-Carr, Elmhurst, USA) containing cooling water. The coil consisted of approximately 6 turns and was housed inside a 30 mL syringe. The ends of the coil were protruding from diagonally opposite holes on the syringe. The top and bottom ends of the coil, which served as the water inlet and outlet for each unit, respectively, were fitted with Y-shaped connectors in a branched configuration to bring water into and out of the coils (Figure 1B). All the coils were connected in parallel, ensuring uniform temperature and flow of cooling water in each unit. The tip of the 30 mL syringe was cut to create an opening to supply a mixture of 30% oxygen-70% nitrogen to the pup during the operation of the cooling unit. Of note, pups were kept in a conscious and non-anesthetized state and spontaneously moved toward the source of oxygen. Thus, the location of the oxygen inlet took advantage of the forward motion of the animal to ensure that the animal's head remained in contact with the coil of cooled water. A peristaltic pump was used to circulate cooled water from the water bath throughout the length of the tubing in each cooling unit and back to the water bath. We optimized the cooling water flow rate, 20 mL/min, and the temperature of the water bath, 19 ± 1°C, to achieve the target brain temperature of 31 ± 1°C. The entire cooling unit containing the rat was kept inside a neonatal incubator maintained at 35.5 ± 0.5°C.

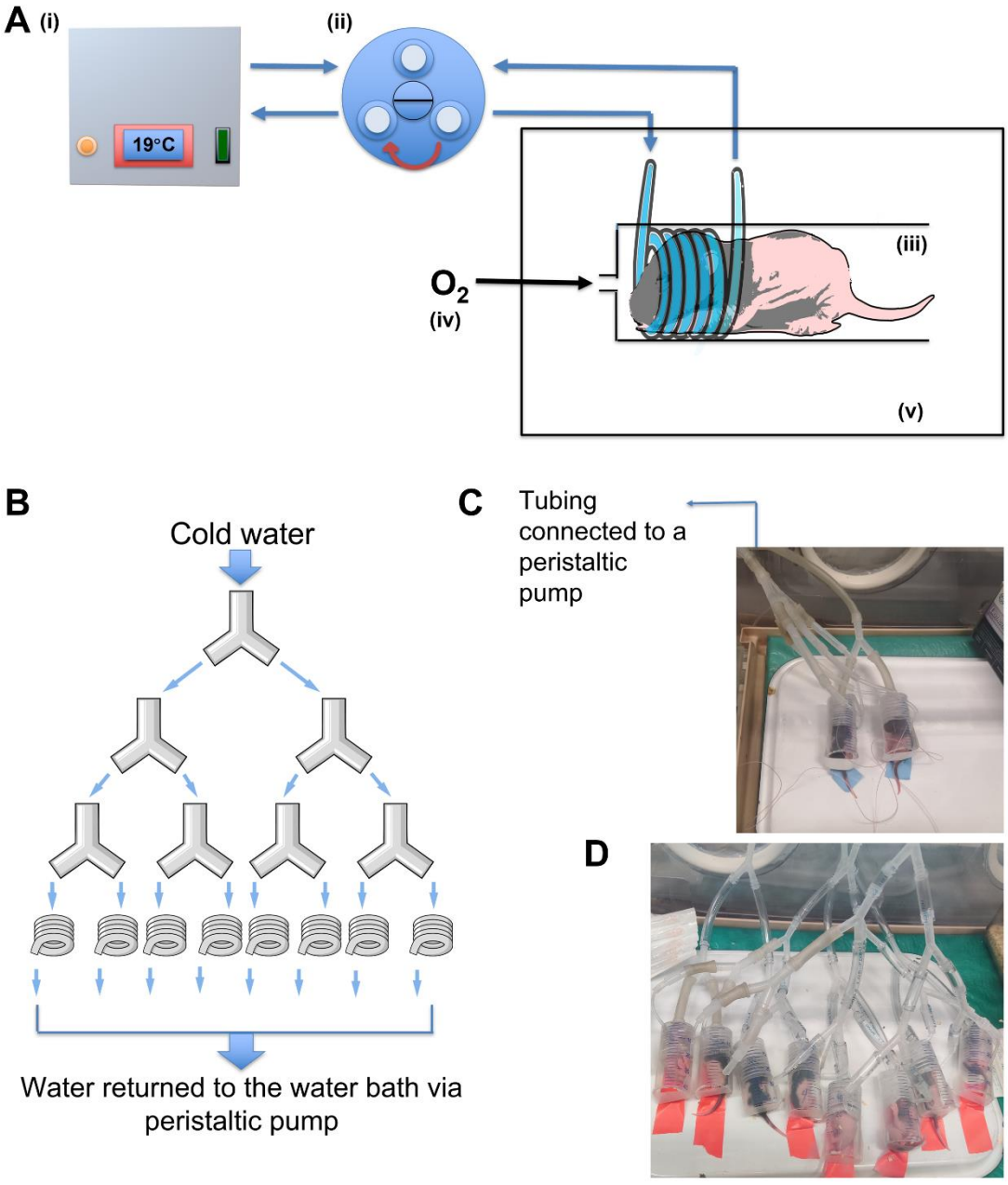


**Figure 2.** The cooling device setup. **(A)** A schematic of the setup. Cooled water (19 ± 1°C, 20 mL/min) drawn from the water bath **(i)** by a peristaltic pump **(ii)** was circulated through the coil of a cooling unit. Each unit consisted of a coil of tubing fitted around the rat's head inside a 30 mL syringe **(iii)**. Oxygen was provided to the animal *via* a port at the tip of each syringe **(iv)**. The cooling unit was in an incubator maintained at 35.5 ± 0.5°C **(v)**. **(B)** The water inflow through the

cooling coils were connected by a branched configuration of Y-shaped connectors to ensure uniform water and temperature distribution across the units. The water outflow from the coils were collected through a similar but converging network of Y-shaped connectors (not shown). **(C)** Two rats were used in Experiment 1 for temperature monitoring and **(D)** up to eight rats could be cooled simultaneously.

### 2.7.2 Experiment 1: Temperature Monitoring

Two thermistor probes (YSI Incorporated, Yellow Springs, USA) were used to measure the temperature of each animal. For core temperature recording, one thermistor probe was inserted into the rectum to a depth of 0.5 mm and secured to the animal's tail using tape. The second thermistor was implanted into the right hippocampus to a depth of 2 mm and at 1.5 mm posterior and 2.2 mm lateral to the bregma and secured in place with dental acrylic. Once the temperature recording was complete, all the animals were euthanized.

### 2.7.3 Experiment 2: Induction of Hypothermia

The PD7 rats subjected to hypoxic-ischemic brain damage as explained in section 2.2, were segregated into normothermic and hypothermic groups, immediately after hypoxia. The normothermic animals were kept in an incubator maintained at 35.5 ± 0.5°C, and for focal hypothermia, the animals were placed in individual cooling units within the incubator. To produce whole-body cooling, the animals were placed in glass jars kept partially submerged in water baths, maintained at 28°C, to reduce the core body temperature to 31 ± 0.5°C. After 24h of normothermia or hypothermia, all animals were returned to their dams. Following the induction of hypoxia-

ischemia and normothermia/hypothermia, all animals were euthanized on PD21. Brains were collected and fresh-frozen in isopentane chilled in an ethanol-dry ice bath. Sections, 14 μm, were cut on a Reichert-Jung Cryocut 1800 cryostat and collected every 0.5 mm. The brain sections were then processed for H&E staining (Appendix A1). Sections were mounted in Cytoseal 60 (Thermo Fisher Scientific, Toronto, Canada). Images were captured using LAS EZ (Leica, Ontario, Canada). ImageJ (version 1.53e; National Institute of Health, Bethesda, USA) was used to measure the area of two and four sections anterior to bregma and the section at bregma for brain volume calculation. The percent damage in each brain section was calculated using the following formula:

$$\%\ \text{Damage} = \frac{\text{Left hemisphere volume} - \text{Right hemisphere volume}}{\text{Left hemisphere volume}} \times 100\%$$

**2.8 Fluorescent imaging using Cyanine5 tagged ELPs**

The biodistribution of ELPs in PD7 rats was analyzed using Olympus OV100/OV110 small animal imaging system. Cyanine5 (Cy5) fluorescent dye was used to label the ELPs (AG)40-(VH4)20 and (AG)80-(VH4)20, since it is most applied for deep tissue imaging and showed better sensitivity at a low concentration (0.01 mg/mL) when injected as a free dye (data not shown). The fluorophore, which is an NHS ester, was allowed to react with the two free amino groups in the ELP under alkaline conditions to result in the cy5 tagged ELP (Appendix A2).

Healthy PD7 rats were intraperitoneally injected with 100μL of Cy5 tagged (AG)80-(VH4)20 and (AG)40-(VH4)24 at 10 mg/kg concentration. Animals were categorized into 3 groups ($n$=2 per group) based on the time point of euthanasia at 4, 24 and 48h post the injection. Following this,

the brain, heart, liver, and kidney were excised immediately after sacrifice and imaged to analyse the localization of ELPs in these organs.

The exposure time was set at 500 ms with 100% intensity. This exposure time gave good images without much saturation. T test was performed to compare the mean counts/PI values between the two animals assuming equal variance. All the extra bright and extra light regions from the organs were measured separately. Approximately, 40 – 80 points were taken and averaged to the get the mean intensity for every organ.

### 2.9 Determination of biocompatibility of ELP constructs using Western blot analysis

To elucidate the biocompatibility of ELPs in the rat model, constructs (AG)80-(VH4)20 and (AG)40-(VH4)24, PD7 pups weighing 12-16 g were injected intraperitoneally with 100 μL of PBS containing 10 mg of ELP per kilogram of body weight. The controls received PBS-only injections at the same injection volume. Organs such as brain, liver, kidney, and heart were collected 48h after the injection and weighed. The homogenized tissue samples were then analyzed by Western blot (Appendix A3) for glial fibrillary acidic protein (GFAP), biomarker for early neuroinflammation (~50kDa), cysteine-aspartic acid protease 3 (caspase-3, Casp3), an apoptotic marker (17/19 kDa) and ionized calcium-binding adapter molecule 1 (Iba1), the marker for macrophage activation (17 kDa).

Each organ was homogenized using tissue protein extraction reagent (TPER) (Thermo Fisher, Carlsbad, USA) containing Pierce Protease Inhibitor (Life Technologies, Burlington, Canada), using 20 mL of solution per gram of tissue, and centrifuged to collect the supernatant. The brain was divided into four quadrants and the cerebellum since it an organ with spatially distinct molecular identities **[122]**. Protein concentration was determined using the Pierce Bicinchoninic Acid (BCA) protein assay kit (Thermo Fisher) according to manufacturer instructions. Antibodies for GFAP (Anti-GFAP, 1:1000, Cell Signaling Technology, Cat# 80788; RRID: AB_2799963), Iba1(Anti-IBA1, 1:1000, Thermo Fisher, Cat# PA5-27436; RRID: AB_2544912), Casp3(Anti-cleaved caspase 3, 1:1000, Cell Signaling Technology, Cat# 9661; RRID: AB_2341188) and loading control (anti-β-Actin, 1:1000, Cell Signaling Technology, Danvers, USA, Cat# 4970; RRID: AB_2223172), were used. The anti-rabbit secondary antibody conjugated to horseradish peroxidase (Sigma-Aldrich, Cat# 07 8K 48 43) was applied at 1:2000 dilution for 1 h at room temperature. Blots were developed using TMB Stabilized Substrate for Horseradish Peroxidase (Promega, Madison, USA) and captured on ImageQuant LAS 4000 (General Electric).

### 2.10 ELP-mediated delivery of dexamethasone to the brain

The ability of (AG)40-(VH4)24 nanoparticles to deliver DEX was investigated by intraperitoneal administration of ELP-DEX solution to PD7 rats (both male and female) subjected to moderate HI damage under hypothermic conditions. Immediately after hypoxia, the rat pups were segregated into two groups: group 1 - HI + normothermia + ELP-DEX treatment ($n$=4) and group 2 - HI + hypothermia + ELP-DEX treatment ($n$=4). The animals in group 2 were placed in the cooling device to effectuate hypothermia while the animals in normothermic group were kept inside an incubator maintained at 35±1°C. Sixty minutes following the initiation of hypothermia, the pups

were intraperitoneally injected with 100µL of PBS (normothermic) or ELP-DEX solution (hypothermic). All the animals were sacrificed 1h after the injection and the organs were collected for further analysis by HPLC.

Due to the unilateral nature of the ischemic damage in the animal model employed, we hypothesized that these high-molecular weight ELP nanoparticles will leverage the increased permeability of the BBB and tend to accumulate more in the right than in the left hemisphere. This has been previously observed by Joseph et al (2018), where the intraperitoneal administration of PLGA-PEG nanoparticles resulted in a 3-fold greater accumulation in the damaged hemisphere than the healthy brain **[123]**. On this account, the analysis of the brain was divided into left and right hemisphere. Concentrations of DEX in all the organs was measured using HPLC following methylene chloride extraction of the drug from the tissue (Appendix A4). The potential analytical loss of DEX during the extraction process was measured in triplicates by correlating it with the amount of internal standard (prednisolone) that was lost during the same procedure. Based on this, the amount of DEX in each type of tissue was calculated from the standard curve and expressed as µg of DEX per gram of tissue (wet weight).

### 2.10.1 HPLC method

The samples were analyzed under a gradient delivery system constituting 2 mM sodium acetate buffer at pH 4.8 (adjusted with glacial acetic acid) and acetonitrile. The acetate buffer was filtered through a 0.2 µm membrane filter prior to use. Reverse-phase HPLC, using a C18 column (4.6 x 250 mm; 5µm particle size; 80Å pore size) was used to determine the concentration of DEX in the

calibration standards. The flow rate of the mobile phase (20-60% acetonitrile in the acetate buffer over 30 minutes) was set at 1mL/min. The eluate containing DEX, and prednisolone (internal standard) was monitored at 241 nm. The detection limit of the HPLC instrument using this method is about 30 ng/mL of DEX in tissue homogenate.

### 2.11 Statistical analysis

The data from the focal hypothermia experiment (experiment 2, section 2.6) and fluorescent imaging experiment were analyzed using Kruskal-Wallis test followed by Dunn's Multiple Comparison *post hoc* test and T-test assuming unequal variances on GraphPad Prism software (version 9.2.0; San Diego, USA).

All the western blots were minimally processed for obtaining uniform contrast using Photoshop (2017.0.0 release; Adobe, San Jose, USA) and quantified using ImageJ (version 1.53e; National Institute of Health, Bethesda, USA). A fixed region of interest (ROI) was used for each band pertaining to the same type of protein and the average staining intensity in each ROI was normalized against that of Actb and then against that of the protein of interest in the control treatment. The Kruskal-Wallis test for statistical analysis was conducted using Graphpad Prism (version 9.2.0; San Diego, USA). A *P*-value below 0.05 was considered statistically significant.

# Chapter 3:

# Results

### 3.1 ELP synthesis

We designed diblock ELPs consisting of a hydrophilic AG domain, with predominantly alanine and glycine alternating as guest amino acids, and a hydrophobic domain containing either lysine, valine, or a combination of valine and histidine as the guest residues. The valine-histidine combination, termed the VH4 domain, has a repeating pattern of one valine and four consecutive histidine as guest amino acids. The amino acid sequences of the expressed and purified ELP are listed in Table 1. ELPs were biosynthesized I n recombinant *E. coli* transformed using an inducible plasmid expression vector. Inverse temperature cycling was conducted to purify the ELPs from the bacterial lysate, and the ELPs were analyzed by gel electrophoresis to visually inspect the molecular weight, as a means to verify chemical composition and biopolymer length, and the purity of the ELPs. Compared to the lysate, there was a reduction in the amount of contaminant peptides in the purified ELPs, and the expected ELP bands were close to the theoretical molecular weight for all the constructs. The molecular weights were also analyzed by mass spectroscopy (Table 1). The mass spectrum of (AG)40-(VH4)24 revealed two distinct peaks; the first peak occurred at a mass to charge ratio approximately half of the second peak, and the mass to charge ratio of the second peak was close to the electrophoretic and theoretical molecular weights of the ELPs (Table 1). We interpret the first and second peaks as doubly and singly charge ELP fragments, respectively. Thus, the electrophoretic and spectroscopic data corroborate to confirm the identity and purity of the ELPs.

### 3.2 Temperature and pH sensitive behavior of ELPs in the presence of DEX

The purified ELP constructs were screened to determine which ELP can form stable nanoparticles at physiological temperature 37ºC and pH 7.4 (pH sensitive ones) and disassemble for drug release below 33ºC and/or in response to a minimal drop in pH to a value between 6.8 and 6. The different ELP concentrations used in this study were selected considering the sensitivity of the DLS instrument and based on previously published work from our lab **[88]**. DEX was used in the formed of DEX saturated PBS that contained ~0.25 mmol/L of DEX.

**Table 1.** List of ELP constructs that have been expressed and purified.

| **ELP system** | **Yield (mg/L)** | **Theoretical Mol.wt (kDa)** | **Mass spectrometry Mol. wt (kDa)** |
|---|---|---|---|
| pH-Responsive: | (Ala-Gly)x-(Val-(His)y)z | | |
| (AG)40-(VH4)20 | 20 | 75138.1641 | 70560.1 |
| (AG)80-(VH4)20 | 27.818 | 105428.2109 | 102204 |
| (AG)40-(VH4)24 | 36.0016 | 83935.9922 | 83822 and 42015 |
| (AG)60-(VH4)24 | 120.94 | 99081.0078 | |
| Hydrophilic-hydrophobic: | (Ala-Gly)x-(Leu)z | | |
| (AG)20-L40 | 10.548 | 34582.4102 | |
| (AG)40-L80 | 55.82 | 68305.8125 | |
| (AG)60-L120 | 45.9 | 102029.2109 | |
| Hydrophilic-hydrophobic: | (Ala-Gly)x-(Val)z | | |
| (AG)20-V40 | 43.7 | 32383.4023 | 32251 |
| (AG)40-V80 | 11.028 | 63907.7930 | 61633 |
| (AG)60-V120 | | 95432.1797 | |

### 3.2.1 (AG)40-L80

(AG)40-L80 at 0.25 mg/mL concentration, showed transition in particle size when heated to 15°C forming ~250 nm sized particles and decreased to ~60 nm upon further heating; the ~60 nm size was maintained up to 45°C. On cooling, the diameter of the particles dropped from ~60 nm to <10 nm between 15 and 20°C (Figure 3).

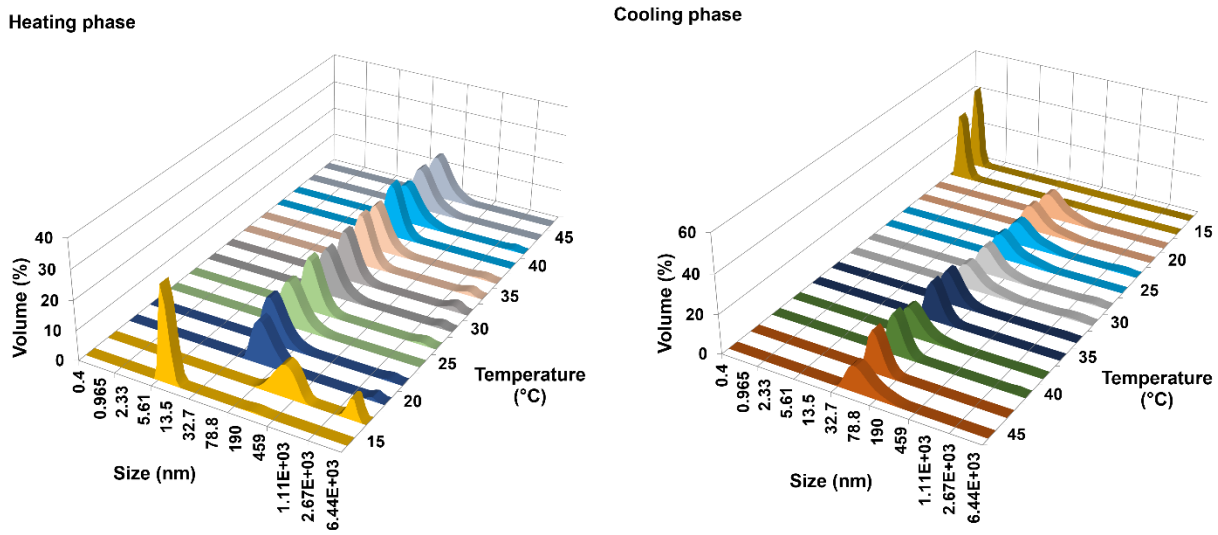


**Figure 3.** The thermal behavior of (AG)40-L80 observed by DLS analysis. The volumetric distribution of particle size was measured over the course of heating from 15 to 45°C and cooling from 45 to 15°C for 0.25 mg/mL of (AG)40-L80.

### 3.2.2 (AG)20-V40 and (AG)40-V80

The results for the behavior of (AG)20-V40 and (AG)40-V80 at concentrations of 0.25 and 0.5 mg/mL, in the presence of DEX, are represented as volumetric distribution of size of the nanoparticles as shown in Figures 2 and 3, respectively. At 0.25 mg/mL, (AG)20-V40 formed nanoparticles of size ~200 nm at around 35°C on heating. On cooling, the diameter dropped from

~200 nm to >10 nm around 40°C (Figure 4A). At 0.5 mg/mL, (AG)20-V40 showed an increase in diameter to ~300 nm at 20°C with no clear decrease in size observed while cooling (Figure 4B). (AG)40-V80 showed transition into particles of size ~140 nm at 25°C at both concentrations of 0.25 and 0.5 mg/mL (Figure 5). The particle size was maintained until 45°C. As the sample was cooled to 15°C, there was no apparent change in diameter at 0.25 mg/mL (Figure 5A) but decreased to ~20 nm at a concentration of 0.5 mg/mL (Figure 5B).

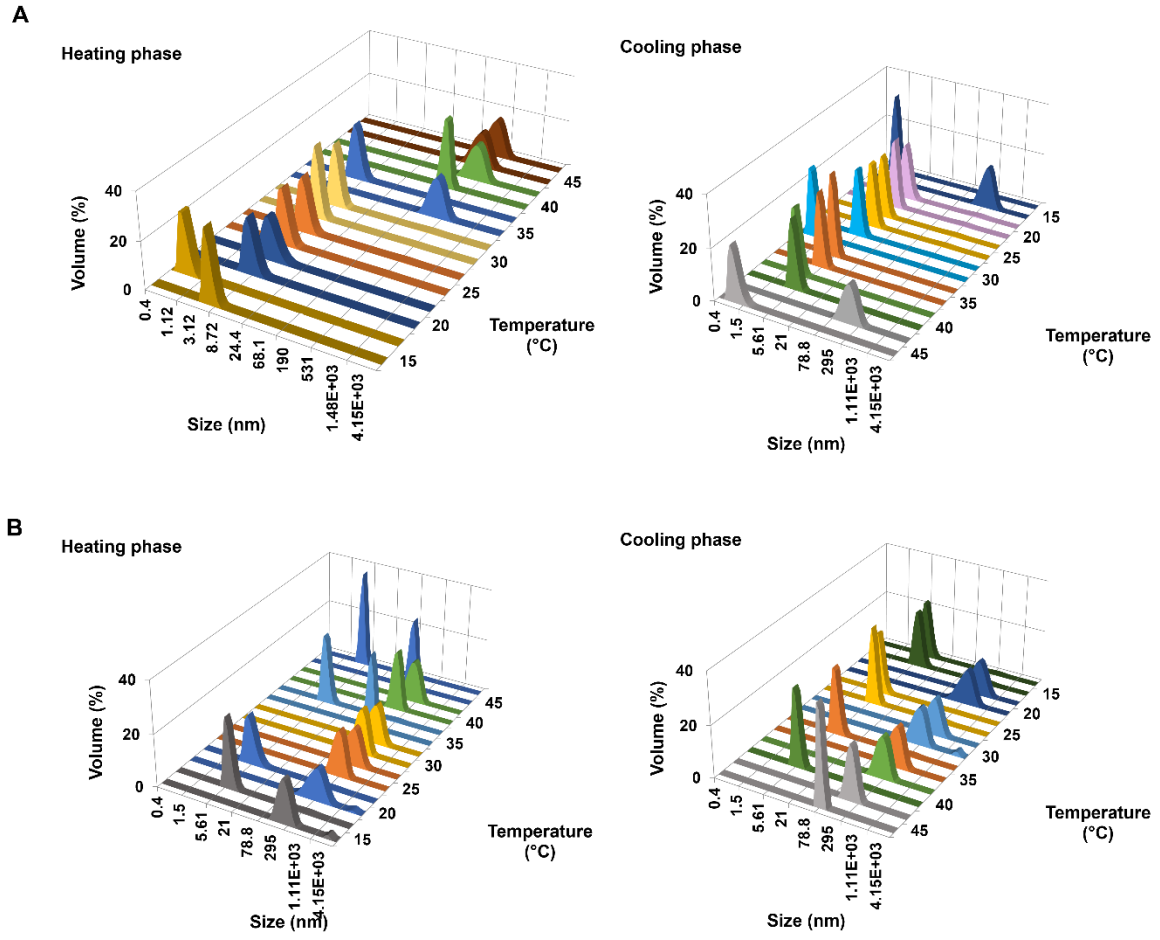


**Figure 4.** The thermal behavior of (AG)20-V40 observed by DLS analysis. The volumetric distribution of particle size was measured over the course of heating from 15 to 45°C and cooling from 45 to 15°C for **(A)** 0.25 mg/mL and **(B)** 0.5 mg/mL of (AG)20-V40.

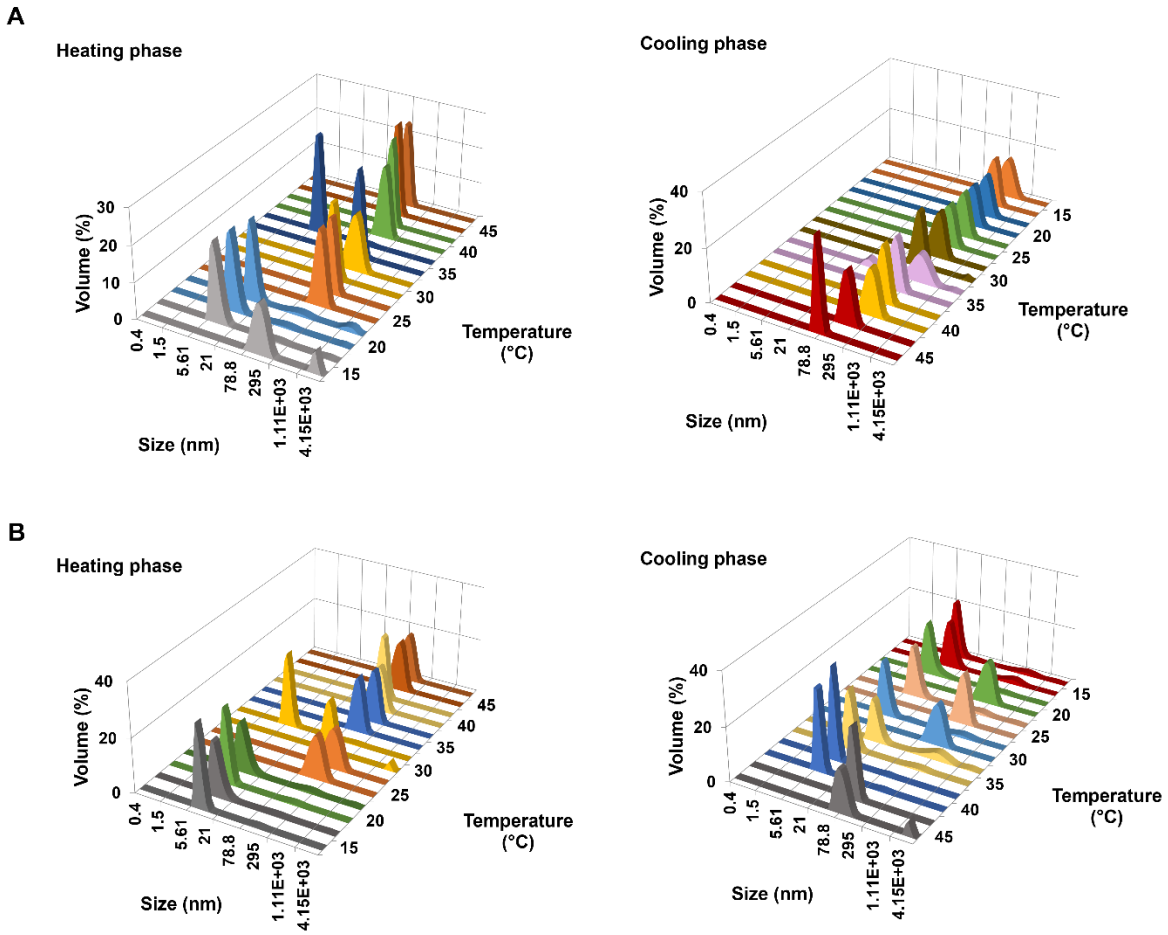


**Figure 5. Figure 3.** The thermal behavior of (AG)40-V80 observed by DLS analysis. The volumetric distribution of particle size was measured over the course of heating from 15 to 45°C and cooling from 45 to 15°C for **(A)** 0.25 mg/mL and **(B)** 0.5 mg/mL of (AG)40-V80.

### 3.2.3 (AG)60-(VH4)24

The assembly and disassembly behavior of (AG)60-(VH4)24 as a function of temperature was analyzed at 0.25, 0.5, and 0.75 mg/mL. At the lowest concentration of 0.25 mg/mL, the particle

size did not change from <10 nm when exposed to increase in temperature from 15 to 45ºC in 5-degree increments. While at 0.5 mg/mL, there was no significant change in particle size (Figure 6A), a marked increase in size occurred from <15 nm to ~80 nm at 30°C and a second transition to particles of size ~500 nm was observed above 40°C (Figure 6B). On lowering the temperature of the sample from 45ºC, a similar trend was observed, with transition to ~50 nm occurring between 40 and 35ºC and complete disassembly to ~10 nm observed below 30ºC.

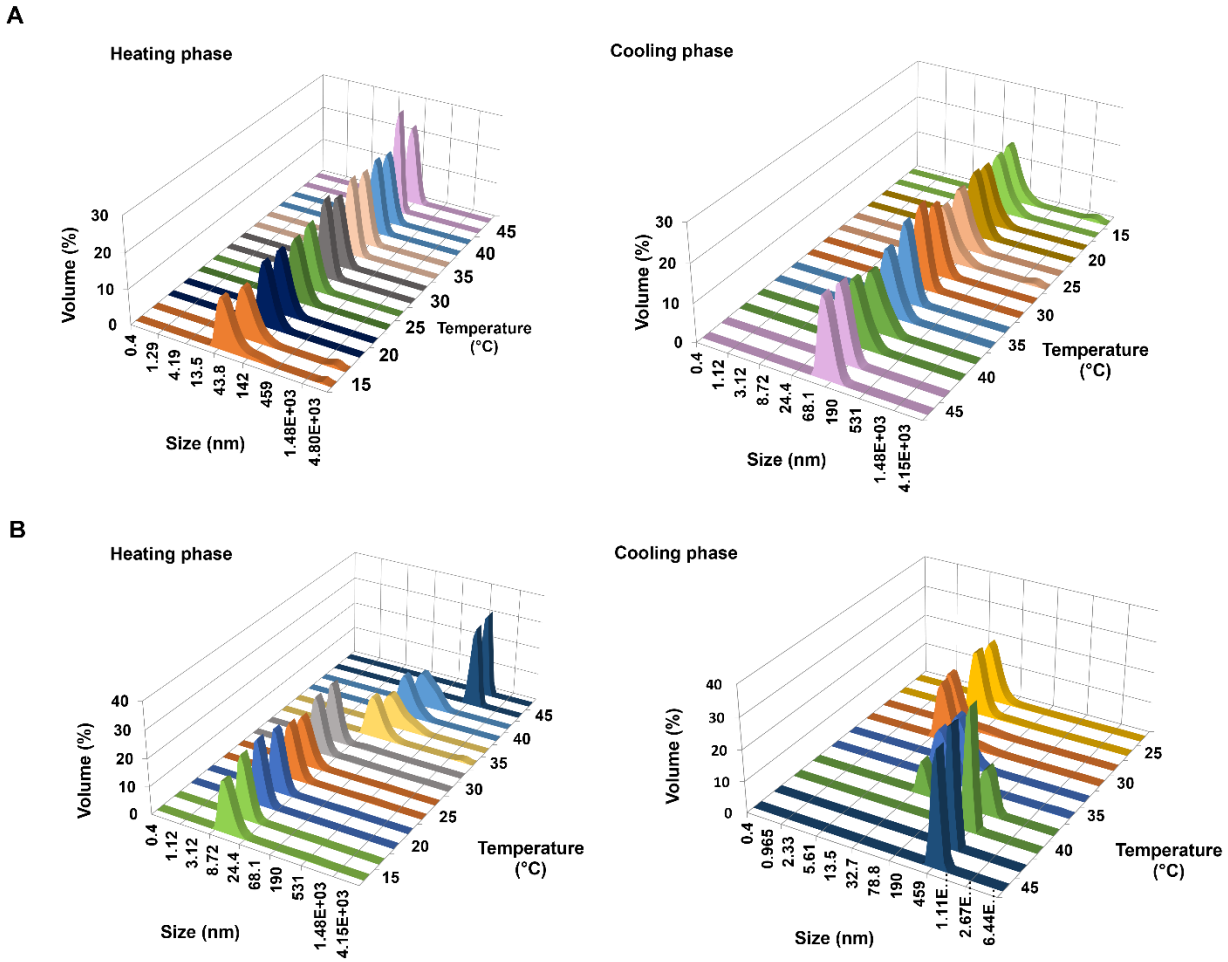

**Figure 6.** The thermal behavior of (AG)60-(VH4)24 was observed by DLS analysis. The volumetric distribution of particle size was measured over the course of heating from 15 to 45°C and cooling from 45 to 15°C for **(A)** 0.5 mg/mL and **(B)** 0.75 mg/mL of (AG)60-(VH4)24.

### 3.2.4 (AG)80-(VH4)20

The temperature-dependent transition of (AG)80-(VH4)20 was observed at 0.25 and 0.5 mg/mL. Direct heating was applied to investigate if particles > 100 nm in size are present at 45ºC. At 0.25 mg/mL, (AG)80-(VH4)20 did not show a clear assembly or disassembly trend, with a very marginal to no change in particle diameters across the temperature gradient (Figure 7A). Cooling the samples of concentrations 0.5 and 0.75 mg/mL, from 45 to 15ºC, showed a slight increase in particle size (Figure 7B and C). The 1 mg/mL samples showed particle size transition from ~125 nm to ~10 nm when the temperature was decreased below 40°C (Figure 7D).

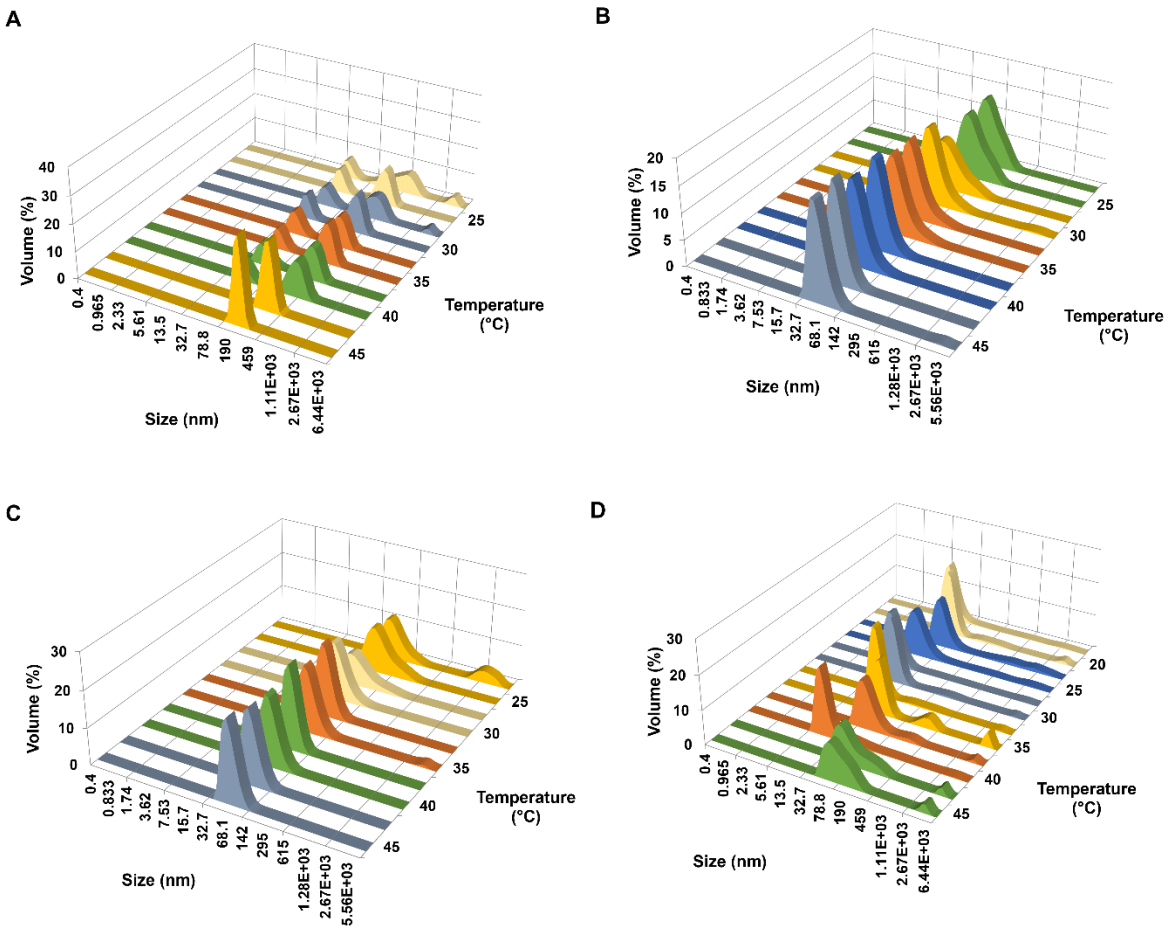


**Figure 7.** The thermal behavior of (AG)80-(VH4)20 observed by DLS analysis. The volumetric distribution of particle size was measured over the course of cooling from 45 to 15°C for **(A)** 0.25 mg/mL, **(B)** 0.5 mg/mL, **(C)** 0.75 mg/mL, and **(D)** 1 mg/mL of (AG)80-(VH4)20.

### 3.2.5 (AG)40-(VH4)20

(AG)40-(VH4)20 transition from ~10 nm into particles ~350 nm above 40ºC at concentration of 0.25 mg/mL. A similar temperature-dependent transition was observed at 0.5 and 0.75 mg/mL (Figure 8A). On cooling below 40ºC, the diameter of the particles returned to the initial size of ~10 nm. At the highest concentration of 1 mg/mL, two different particle size transitions from 10

to ~45 nm above 30ºC and from ~45 to ~250 nm above 40ºC, were observed, with reverse trend during cooling (Figure 8B). The disassembly of these particles as a function of pH is shown in (Figure 9). At 0.75 mg/mL, pH-triggered disassembly of (AG)40-(VH4)20 was observed when the pH was lowered from 7.4 to 6.4, causing a decrease in particle size to less than 50 nm (Figure 9). On further lowering the pH to 6.2, nanoparticle formation did not occur over the range of 15-45ºC (Figure 9).

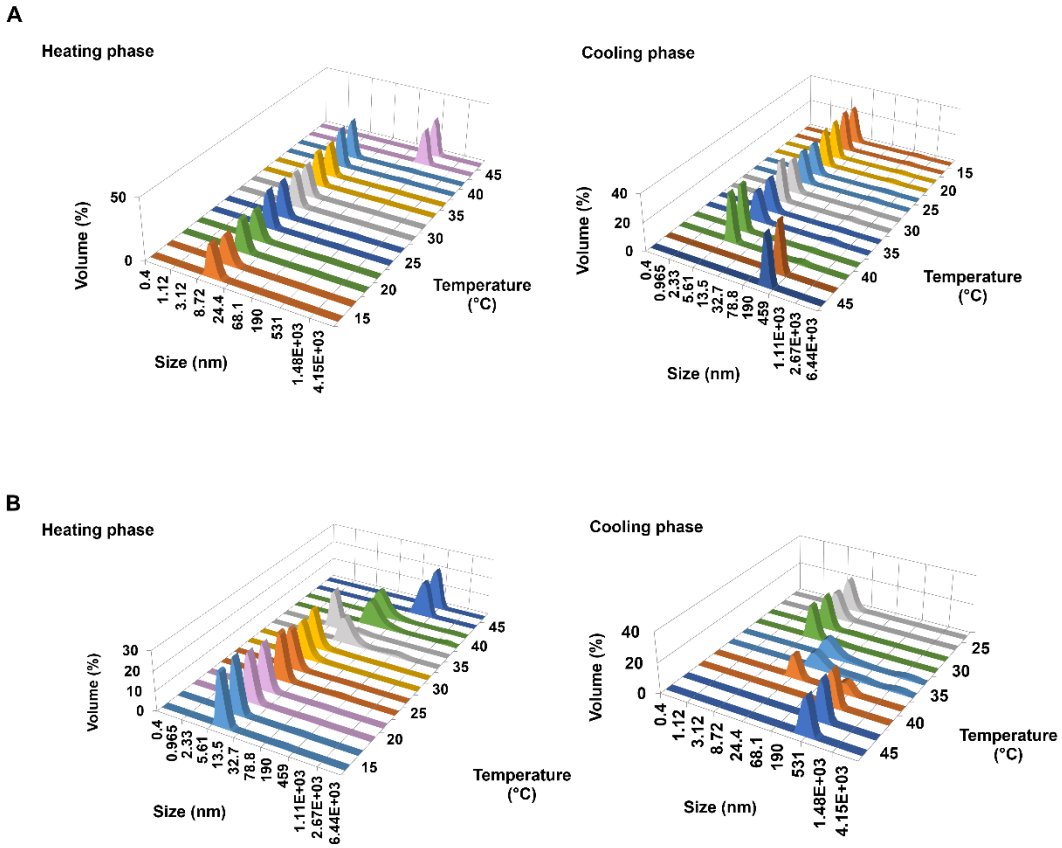


**Figure 8.** The thermal behavior of (AG)40-(VH4)20 was observed by DLS analysis. The volumetric distribution of particle size was measured over the course of heating from 15 to 45°C and cooling from 45 to 15°C for **(A)** 0.75 mg/mL and **(B)** 1 mg/mL of (AG)40-(VH4)20.

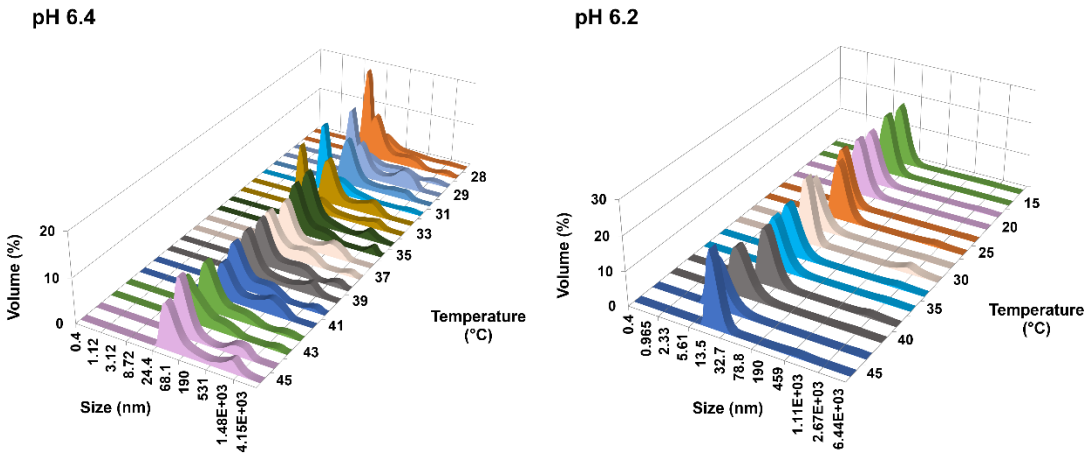


**Figure 9.** Results from DLS analysis. pH-induced disassembly of (AG)40-(VH4)20 at 0.75 mg/mL at pH 6.4 and 6.2, represented in terms of volumetric distribution of the nanoparticles.

### 3.2.6 (AG)40-(VH4)24

At pH 7.4, construct (AG)40-(VH4)24 demonstrated an increase in particle size from ~1 nm to ~250 nm above 37ºC, when temperature of the solution was gradually increased from 15 to 45ºC, at a concentration of 0.25 mg/mL. On cooling, the diameter of the particles dropped to <20 nm below 34°C (Figure 10). Similar trend was observed at a higher concentration of 0.5 mg/mL where nanoparticles ~400 nm formed on directly raising the solution temperature to 45ºC. On lowering the pH to 6.4 and 6, at 0.25 mg/mL, it can be observed in Figure 11A, that the nanoparticles became unstable and underwent disassembly below 34°C, with complete dissociation to <10 nm at pH 6 across all temperatures. Similarly, at 0.5 mg/mL, the disassembly temperature was lowered to nearly 32°C, on decreasing the solution pH to 6.2 (Figure 11B).

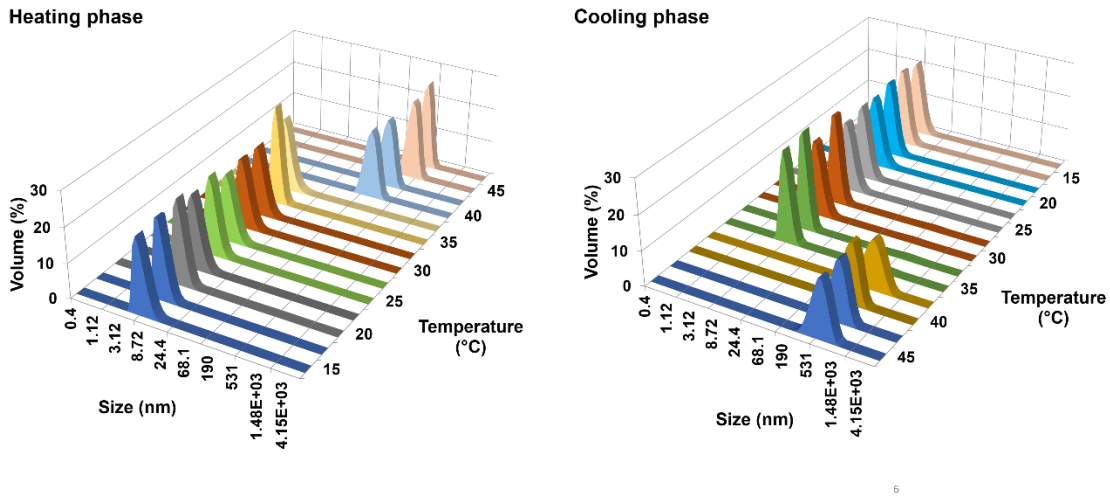


**Figure 10.** The thermal behavior of (AG)40-(VH4)24 observed by DLS analysis. The volumetric distribution of particle size was measured over the course of heating from 15 to 45°C and cooling from 45 to 15°C for 0.25 mg/mL of (AG)40-(VH4)24.

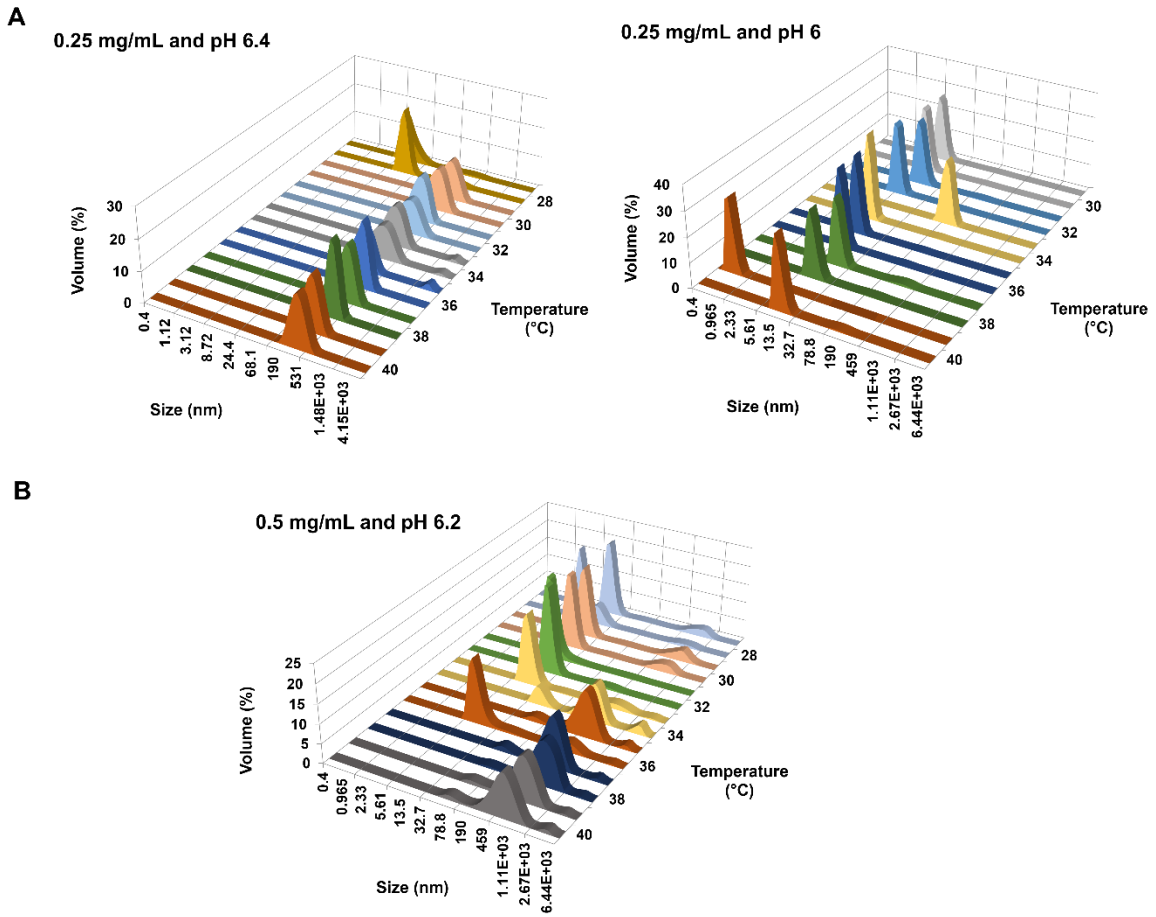


**Figure 11.** Results from DLS analysis. pH-induced disassembly of (AG)40-(VH4)24 at **(A)** 0.75 mg/mL and **(B)** 0.5 mg/mL, represented in terms of volumetric distribution of the nanoparticles.

### 3.3 Encapsulation efficiency and effect of DEX encapsulation on nanoparticle stability

The encapsulation efficiency of (AG)40-(VH4)24 was determined to be 1.3 ± 0.6 % of concentration of DEX saturated PBS (Table 2). The data obtained were from three replicates for each time point. The amount of DEX that can be loaded into (AG)40-(VH4)24 at 0.25 mg/mL of the ELP is 1.27 µg. The encapsulation efficiency was calculated over 3 days to determine if the nanoparticles retain the same amount of DEX during this period, a measure reflective of the

stability of the particles. It was observed (Table 2) that encapsulated DEX decreased to the point of being below the level of detection (<LOD) after two days in solution, suggesting particles need to be freshly made prior to application.

**Table 2.** Encapsulation efficiency and nanoparticle stability of (AG)40-(VH4)24

| Days post-encapsulation | % of encapsulated DEX |
|---|---|
| **0** | 1.3 ± 0.6 |
| **1** | 0.7 ± 0.242 |
| **2** | Below LOD |
| **3** | Below LOD |

### 3.4 Induction of focal brain hypothermia

Existing designs for focal cooling use chilled water as the heat transfer fluid that is circulated in proximity to the head. Thus, we designed an apparatus to induce moderate hypothermia in the neonatal rat brain, where the rat head was fitted within a coil of tubing carrying 20 mL/min of cold water. The cooling units operated inside an incubator maintained at 35.5 ± 0.5°C to minimize the loss of core body heat. To evaluate the performance of the cooling units, we monitored the brain and core body temperature of PD7 rats over the course of 16.5 hours of cooling (Figure 12). The temperature of the water entering the coil was set originally at 28°C, corresponding to the water temperature used for immersive, whole-body cooling of rats, and was optimized to 19 ± 1°C to obtain the target brain temperature, 31°C. It took less than 15 min. for the brain temperature to drop below 33°C and, after 4h, was maintained at an average of 31 ± 1°C through the remainder of the experiment. The core temperature decreased from approximately 36.7°C initially to 33.0°C at the end of the cooling period. A temperature differential of about 3.2°C was steadily maintained

between the brain and core. Therefore, the cooling device is able to selectively induce moderate cooling of the brain.

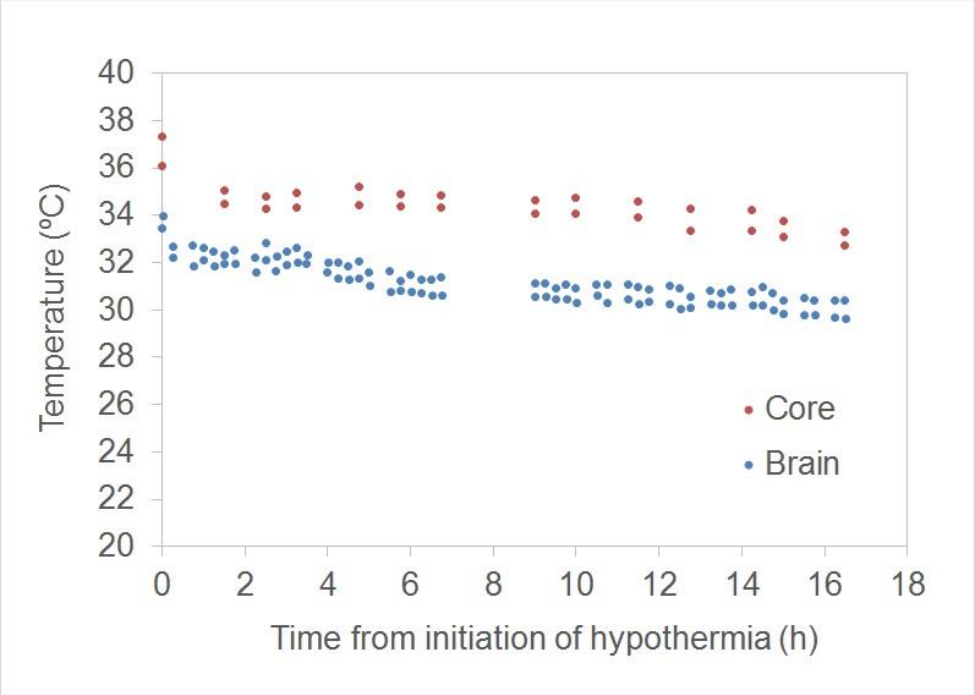


**Figure 12.** Core body and brain temperature profiles during the operation of the cooling device. Temperature probes were inserted into the rectum and right hippocampus of PD7 rats ($n$ = 2 pups) to monitor the core body and brain temperature, respectively. Each dot represents a reading from one pup. The brain temperature started to decrease within 15 min. from the beginning of cooling. A temperature difference of about 3.2°C was maintained between the brain of the animal and the rectal (core) temperature.

### 3.5 Neuroprotection by the cooling device

To validate the therapeutic potential of the cooling device, PD7 rats were subjected to hypoxic-ischemic damage and subsequently divided into three groups of temperature treatment: normothermic control, focal hypothermia, and whole-body hypothermia. No anesthesia was

administered. The baseline core body temperature among all groups was 36 ± 1°C. Normothermic animals were incubated at 35.5 ± 0.5°C, and for focal hypothermia, the animals were placed in individual cooling units within the incubator. For whole-body cooling, the core body temperature was decreased to 31 ± 0.5°C. The duration of the hypothermic treatment was 24h.

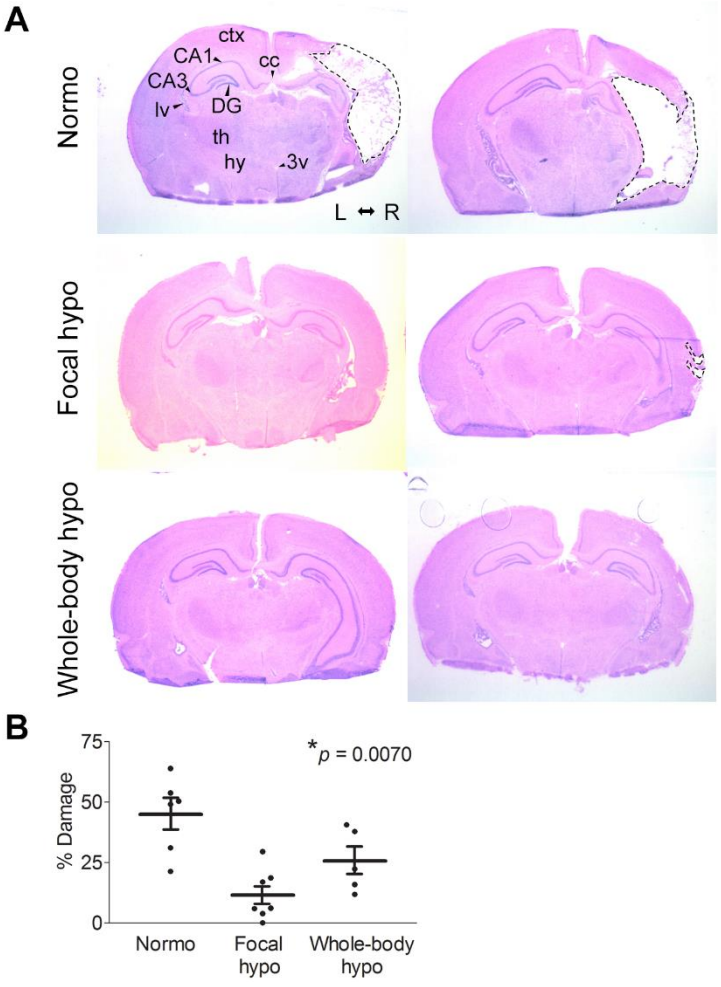


**Figure 13.** Treatment by the cooling device reduced the extent of brain atrophy. Hypoxic-ischemic injury was induced in PD7 pups, followed by 24h of hypothermic treatment, and assessed on PD21 by hematoxylin and eosin staining of coronal brain sections. Hypothermic treatment was carried out as focal hypothermia within a cooling unit or by whole-body cooling. **(A)** Representative sections from two brains are shown from each treatment group. The dashed lines indicate the

regions of lost brain tissue. **(B)** The percent brain damage after focal hypothermia ($n$ = 7 pups) and whole-body hypothermia ($n$ = 5 pups) was compared to that of the normothermic control ($n$ = 6 pups).The horizontal line and error bars represent the mean ± standard error of the mean. *Significantly different *versus* normothermic treatment, $p$ = 0.007 by Kruskal-Wallis test followed by Dunn's multiple comparison *post hoc* test. Abbreviations: 3v, third ventricle; cc, corpus callosum; ctx, cerebral cortex; DG, dentate gyrus; hy, hypothalamus; L, left; lv, lateral ventricle; R, right; th, thalamus.

The extent of brain damage on PD21 was assessed by histological examination of the brain tissue using hematoxylin and eosin staining. The location of the hypoxia-ischemia-induced lesion was in the right cerebral hemisphere, ipsilateral to the ligated right carotid artery. The brains of normothermic animals, which experienced the most damage, had characteristic porencephalic cyst (Figure 13A). In most animals across the hypothermic groups, the hippocampus remained intact and ventricle enlargement was relatively mild compared to the normothermic group. Furthermore, the percent brain damage was quantified and compared among the normothermic and hypothermic groups. The normothermic group had significantly greater brain tissue loss in comparison to the hypothermic group where cooling was applied to the head (Figure 13B). Notably, both focal and whole-body cooling were similarly neuroprotective. Altogether, the data confirm the effectiveness of the cooling device to decrease the temperature of the neonatal brain for a therapeutic outcome.

### 3.6 Biodistribution of ELPs

The end-point fluorescent images of the organs such as the brain, heart, liver and kidneys, from the animals that were injected with Cy5 tagged ELPs (10mg/kg) (AG)40-(VH4)20, (AG)80-

(VH4)20, showed the presence and distribution of the ELPs (Figure 14 A and B). There was a significant difference observed in the mean pixel intensity between the PBS injected and ELP injected animals across almost all the organs at 4h (Figures 15 and 16), 24h (Figures 17 and 18), and 48h (Figures 19 and 20). Liver and kidney showed the highest fluorescence intensities, followed by the heart and the brain. The significantly higher signal intensity in the brains of animals that administered with tagged ELP over the controls confirmed the localization of ELPs in the brain.

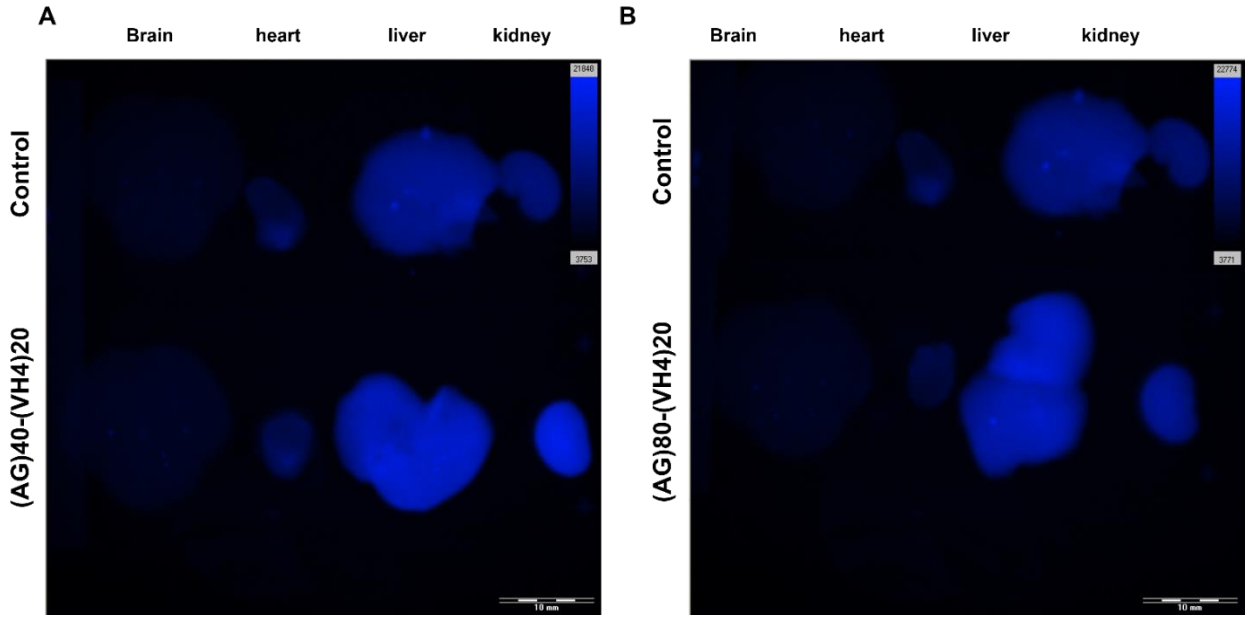


**Figure 14.** The localization of Cy5-labelled ELPs. Representative images of organs from rats that were intraperitoneally injected with 10 mg/kg of Cy5 tagged **(A)** (AG)40-(VH4)20 and **(B)** (AG)80-(VH4)20 and euthanized 4h after the injection.

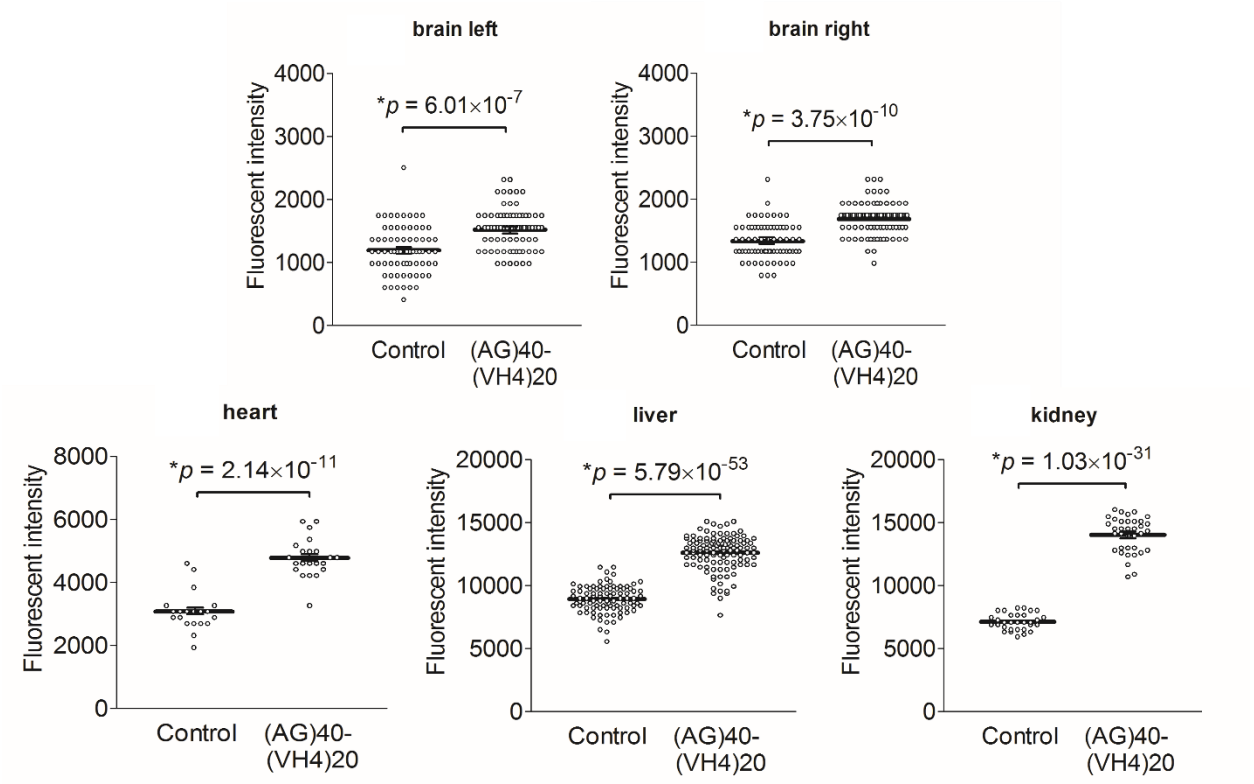


**Figure 15.** Dot plots of end point fluorescent images of animal injected with Cy5 tagged (AG)40-(VH4)20 and euthanized at 4h post injection. Each point on the dot plots represents the fluorescent intensity of a sample point corresponding to a single pixel on the image. The horizontal line and error bars denote the mean ± SEM. *Statistical significance between the control and ELP-treated groups were analyzed by t-test, and the *p*-values are indicated.

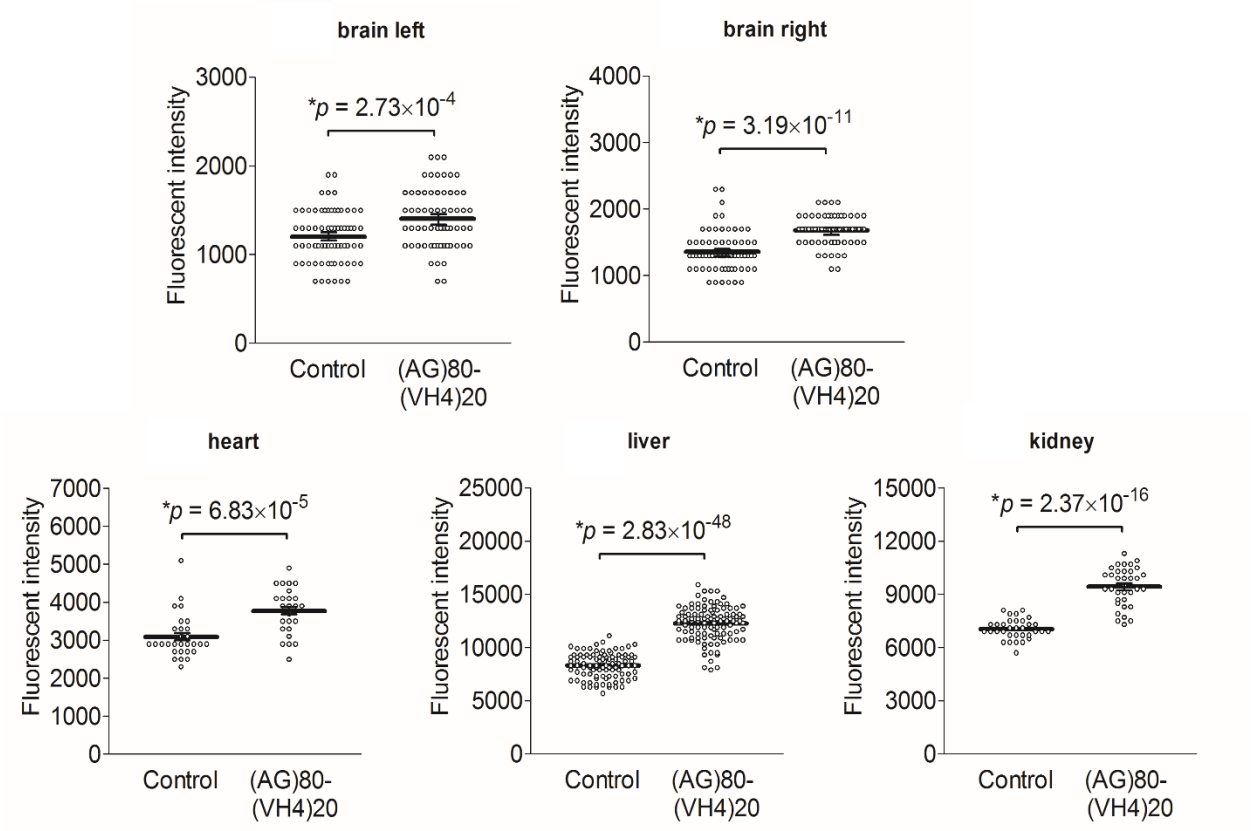


**Figure 16.** Dot plots of end point fluorescent images of animal injected with Cy5 tagged (AG)80-(VH4)20 and euthanized at 4h post injection. Each point on the dot plots represents the fluorescent intensity of a sample point corresponding to a single pixel on the image. The horizontal line and error bars denote the mean ± SEM. *Statistical significance between the control and ELP-treated groups were analyzed by t-test, and the *p*-values are indicated.

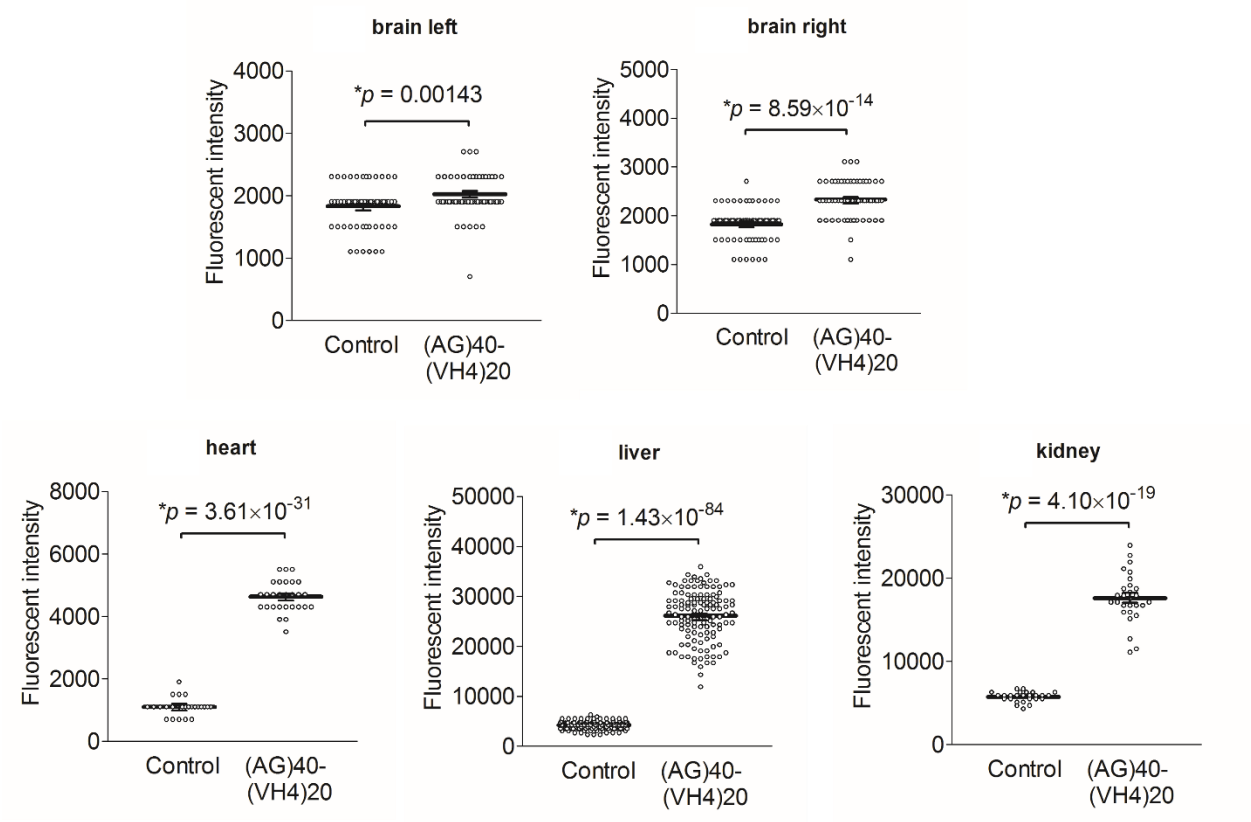


**Figure 17**. Dot plots of end point fluorescent images of animal injected with Cy5 tagged (AG)40-(VH4)20 and euthanized at 24h post injection. Each point on the dot plots represents the fluorescent intensity of a sample point corresponding to a single pixel on the image. The horizontal line and error bars denote the mean ± SEM. *Statistical significance between the control and ELP-treated groups were analyzed by t-test, and the *p*-values are indicated.

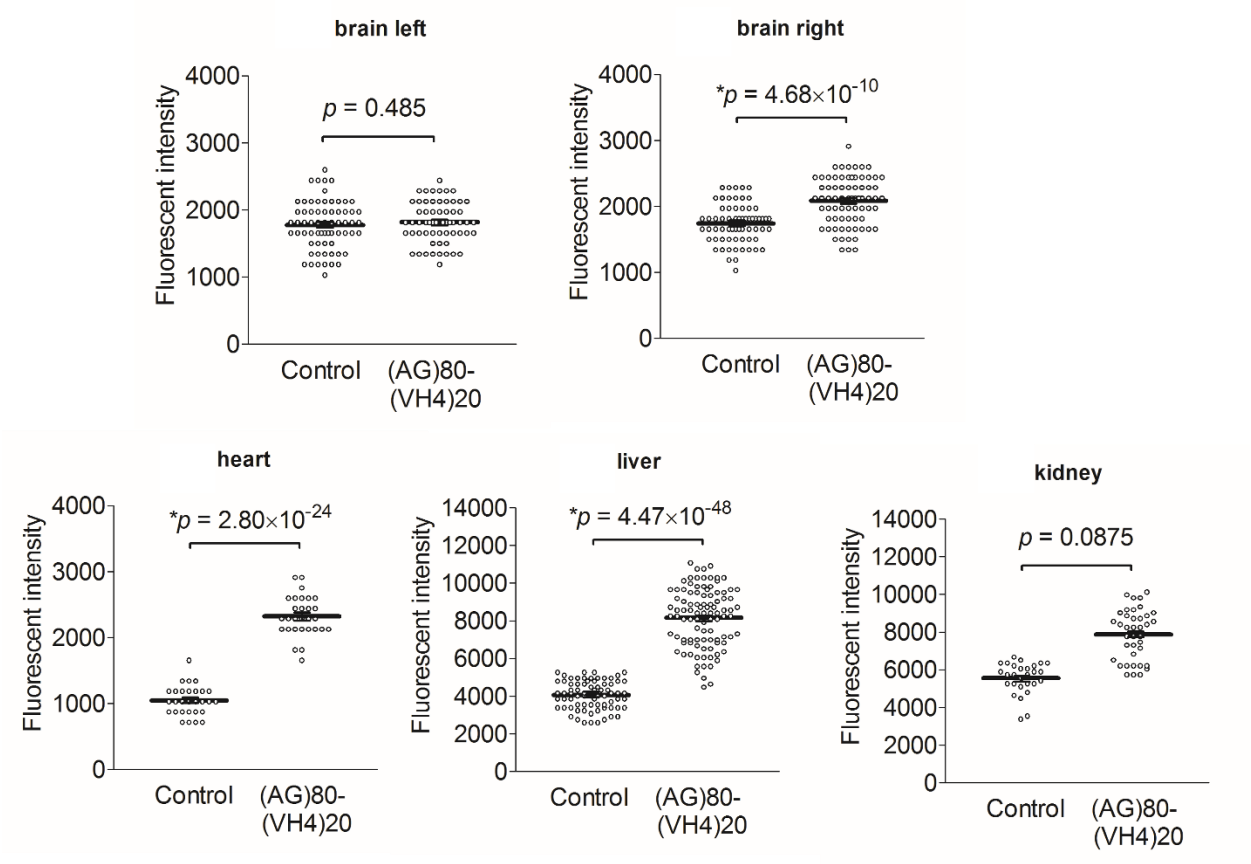


**Figure 18.** Dot plots of end point fluorescent images of animal injected with Cy5 tagged (AG)80-(VH4)20 and euthanized at 24h post injection. Each point on the dot plots represents the fluorescent intensity of a sample point corresponding to a single pixel on the image. The horizontal line and error bars denote the mean ± SEM. *Statistical significance between the control and ELP-treated groups were analyzed by t-test, and the *p*-values are indicated.

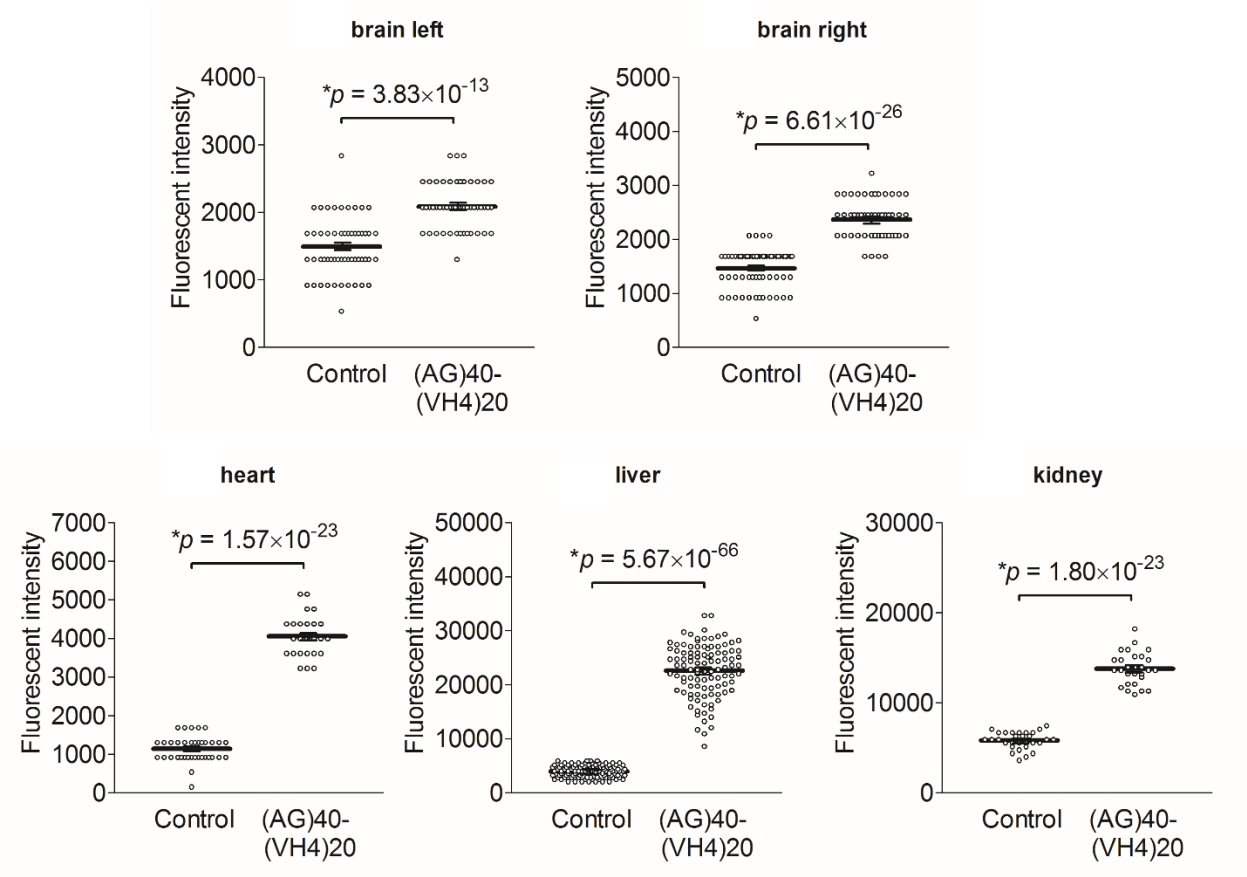


**Figure 19.** Dot plots of end point fluorescent images of animal injected with Cy5 tagged (AG)40-(VH4)20 and euthanized at 48h post injection. Each point on the dot plots represents the fluorescent intensity of a sample point corresponding to a single pixel on the image. The horizontal line and error bars denote the mean ± SEM. *Statistical significance between the control and ELP-treated groups were analyzed by t-test, and the *p*-values are indicated.

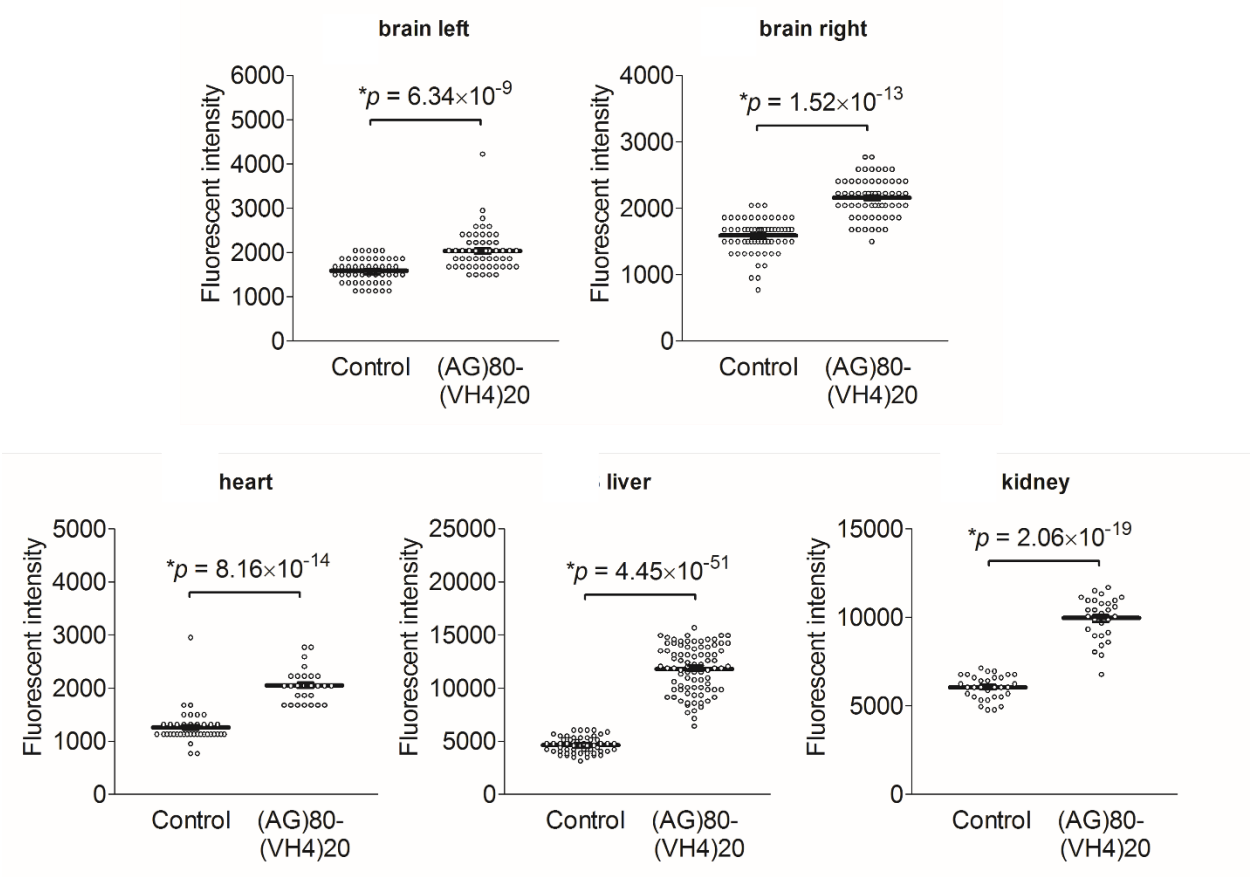


**Figure 20.** Dot plots of end point fluorescent images of animal injected with Cy5 tagged (AG)80-(VH4)20 and euthanized at 48h post injection. Each point on the dot plots represents the fluorescent intensity of a sample point corresponding to a single pixel on the image. The horizontal line and error bars denote the mean ± SEM. *Statistical significance between the control and ELP-treated groups were analyzed by t-test, and the *p*-values are indicated.

### 3.7 *In vivo* biocompatibility of ELPs

To screen for the biocompatibility of ELPs in a neonatal model, ELPs were injected intraperitoneally into PD7 rats at a dose of 10 mg/kg body weight. Tissue samples were weighed

two days after ELP administration and also assayed by Western analysis for cysteine-aspartic acid protease 3 (caspase-3, Casp3) and ionized calcium-binding adapter molecule 1 (Iba1) as markers for apoptosis and macrophage activation, respectively. A chief apoptotic effector, Casp3, is proteolytically activated to yield 17/19 kDa subunits. Iba1 is a 17 kDa EF hand protein whose expression is upregulated in response to tissue damage. There was constitutive Casp3 cleavage and Iba1 expression in the liver (Figure 21A), and ELP treatment did not significantly upregulate these markers above basal levels (Figure 21A). In contrast, Casp3 fragments were not observed in the kidney (Figure 21B) or heart (Figure 21C), and Iba1 expression in the heart was similar among the control and ELP-injected pups (Figure 21C).

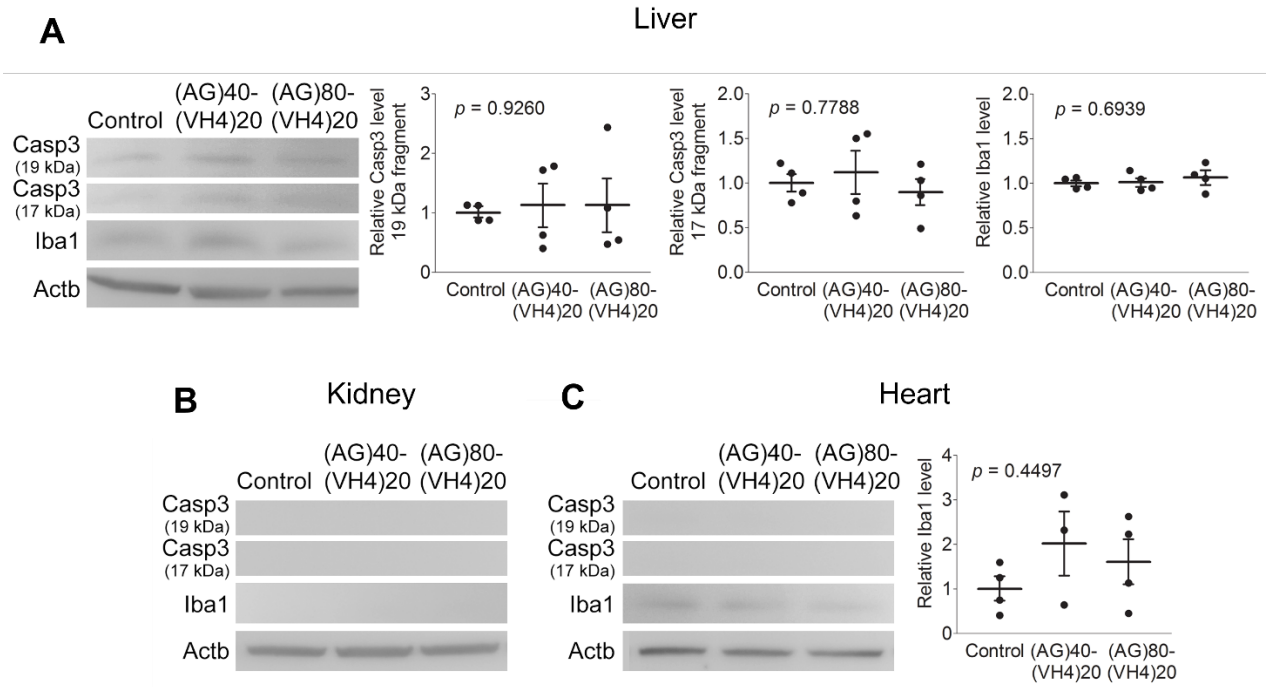


**Figure 21.** Western analysis of heart, liver, and kidney. Protein blots of markers of cell death and inflammation in the **(A)** liver, **(B)** kidney, and **(C)** heart of rats after ELP injection. The band intensity of activated Casp3 fragments (17/19 kDa) and Iba1, where detectable, was normalized against that of the loading control, Actb.

The detection of ELPs in the brain prompted us to look for evidence of neuroinflammation. The brain is a particularly complex organ because of the spatially distinct molecular identities **[122]**. Hence, the analysis of the brain was divided into cerebral quadrants and the cerebellum. Of note, in addition to Casp3 and Iba1, Western analysis on brain samples also involved glial fibrillary acidic protein (Gfap, 50 kDa) as an early marker of neuroinflammation **[124]**. ELP treatment did not significantly affect the weight of the brain or subsections of the brain (Figure 22). Casp3 fragments and Iba1 were not detected in the cerebrum (Figure 22A). The level of Gfap expression was comparable among control and ELP-injected pups for all cerebral quadrants (Figure 22A). Similarly, the cerebellum did not have observable levels of Casp3 cleavage or Iba1 expression (Figure 22B) and had no significant difference in Gfap expression among the control and ELP treatments (Figure 22B). Altogether, the data indicate no evidence of apoptosis, macrophage activation, or neuroinflammation in these organs following ELP administration.

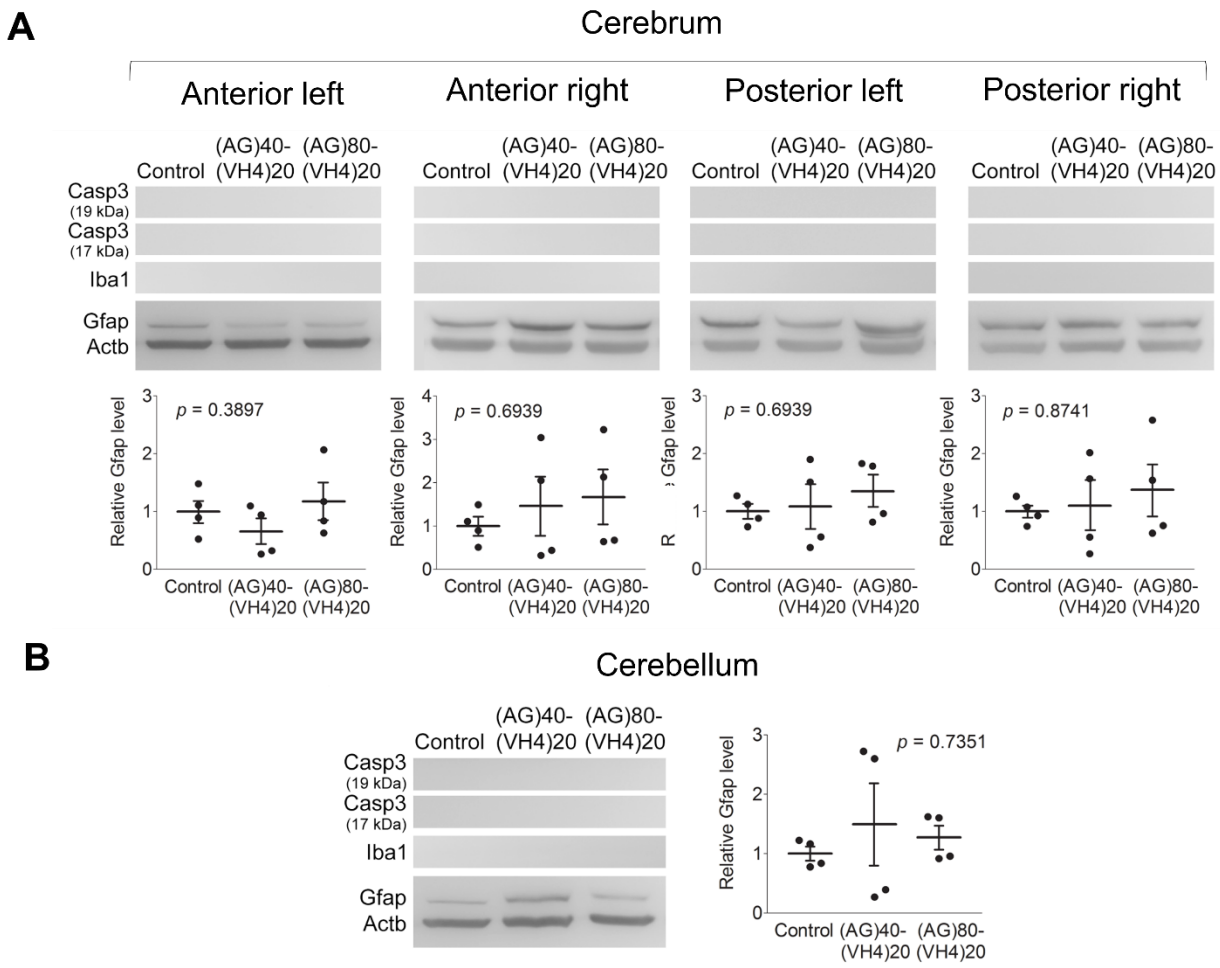


**Figure 22.** Western blot analysis of the brain. Protein blots of markers of cell death and inflammation in the **(A)** quadrants of cerebrum and **(B)** cerebellum after ELP injection. The band intensity of activated Casp3 fragments (17/19 kDa), Iba1 and Gfap, where detectable, was normalized against that of the loading control, Actb.

### 3.8 *In vivo* release of dexamethasone in the brain

The amounts of DEX in different organs such as the brain, heart, liver, and kidney were measured for both groups, 60 mins after the intraperitoneal administration of DEX-containing (AG)40-(VH4)24 nanoparticles into pups with HI damage. The unknown quantities were calculated from

a calibration curve obtained individually for every organ. The peak areas were linearly related with the known concentrations (between 0.5 and 10 µg/mL (Figure 23)) of DEX that were prepared using the homogenate from the corresponding organ. The high R squared value of ~0.999 represents the linearity of the calibration curve. The percent of DEX lost during methylene chloride extraction was 60± 1.2%.

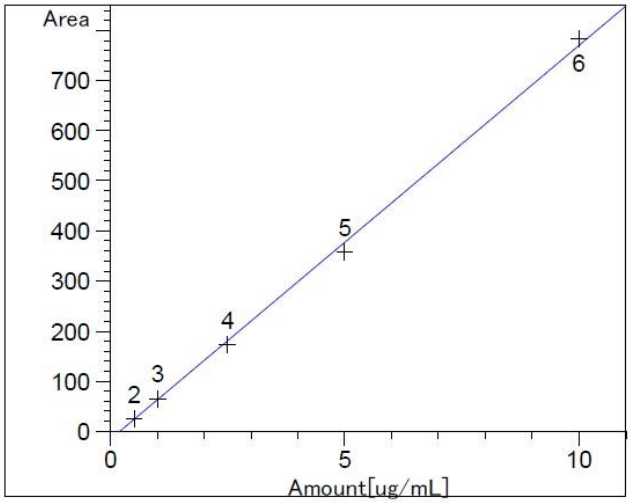


**Figure 23.** Calibration curve of DEX standards prepared from brain homogenate.

Table 3. shows the quantification of DEX detected and measured in the brain from 4 animals, expressed as µg of DEX per gram of wet tissue. DEX was not detected in any of the organs from the rats besides the brain.

**Table 3.** DEX quantification in the brain tissue from rats injected with ELP-DEX solution.

| Sample | Amount (µg/mL) | Amount of DEX per mass of tissue ((µg/g) |
|---|---|---|
| Rat 1 left hemisphere – normothermic | Below LOD | - |
| Rat 1 right hemisphere – normothermic | Below LOD | - |
| Rat 2 left hemisphere – hypothermic | 0.283147 | 0.397 |
| Rat 2 right hemisphere – hypothermic | 0.432560 | 0.485 |
| Rat 3 left hemisphere – normothermic | Below LOD | - |
| Rat 3 right hemisphere – normothermic | 0.272819 | 0.3883 |
| Rat 4 left hemisphere – hypothermic | Below LOD | - |
| Rat 4 right hemisphere - hypothermic | Below LOD | - |

# Chapter 4:

# Discussion

### 4.1 ELP synthesis

ELP expression in recombinant *E. coli* was induced by IPTG. Inverse temperature cycling, a process that extracts ELPs by exploiting their reversible phase transition property was employed to purify ELPs from bacterial lysate. The ELPs described in this study are composed of a hydrophilic domain containing alanine and glycine in the ratio of 1:1, in the guest amino acid position and a hydrophobic domain that contains either leucine, valine or valine and histidine in the ration of 1:4 as the guest residues. Both the hydrophilic and hydrophobic blocks together constitute an ELP diblock copolymer. During the purification of leucine and valine containing ELP diblock constructs, sodium chloride was added up to a final concentration of 5 M while performing the hot spin at 40°C to extract the ELP from the sample via aggregation. This is because both leucine and valine are highly hydrophobic amino acids, compared to the valine and uncharged histidine combination in the hydrophobic domain of the other pH-sensitive constructs (in accordance with Urry's hydrophobicity scale). ELPs containing guest amino acids with high hydrophobicity have the tendency to transition at or below room temperature (ref) and therefore are likely removed from the solution when centrifuging to eliminate insoluble cell debris. This could have resulted in their lower concentration, which in turn entails more salt to bring about molecular crowding to drive aggregation via hydrophobic interactions.

.

### 4.2 ELP assembly and disassembly in the presence of DEX

Diblock ELPs are designed such that the hydrophobic domain drives nanoparticle assembly because of increase in its surface tension during the heating process **[91]**. The hydrophilic domain forms a hydrated corona around the hydrophobic core to suspend the nanoparticle in solution. Moreover, the physicochemical properties of the guest amino acid in the ELP sequence allows the ELP to undergo phase transition in response to specific environmental cues. Among the proteinogenic amino acids, histidine in particular has a p$K_a$ nearest to pH 7.4 and is thus expected to ionize within a narrow, physiologically relevant pH range. Therefore, the incorporation of histidine residues in the hydrophobic domain confers pH responsiveness to the ELP **[86]**. The injected ELPs remain as nanoparticles at the normal physiological pH 7.4, but the local acidic environment of injured brain tissue, around pH 6.4, triggers the ionization of histidine residues and leads to the overall disassembly of the ELP nanoparticle.

The concentration of (AG)40-(VH4)24 affected the size of the nanoparticles when the temperature was increased from 15 to 45 degrees. While at 0.25 mg/mL, particle size remained between 200-300 nm, increase in the concentration to 0.5 mg/mL resulted in the formation of ~450 nm sized particles. Concentration also had an impact on pH-induced disassembly of this construct. A reduction in pH from 7.4 to 6.4, lowered the transition temperature from 34ºC to less than 30ºC at 0.25 mg/mL, respectively. Nanoparticle assembly did not occur at this concentration when the pH was dropped from 7.4 to 6. At 0.5 mg/mL, the particles disassembled below 34ºC at pH 6.4 and below 38ºC at pH 6. The difference in dissociation temperatures between 0.25 and 0.5 mg/mL at pH 6.4, might be attributed the lower mass concentration of (VH4) at 0.25 mg/mL; a greater

fraction of uncharged histidine residues would have been protonated compared to 0.5 mg/mL at this pH value.

The decrease in length of the ELP by four units of VH4 in (AG)40-(VH4)20 increased the transition temperature of this construct at which nanoparticle assembly occurs. A steady increase in particle size from ~350 nm to ~450 nm was observed when the concentration was increased from 0.25 to 1 mg/mL. An interesting transition emerged at the highest concentration of 1 mg/mL: two different particle size transitions from 10 to ~45 nm above 30ºC and from ~45 to ~250 nm above 40ºC, was observed. A similar behavior in reverse was demonstrated during cooling, where the transition to ~50 nm occurred when the sample was cooled below 40ºC and a subsequent drop to 10 nm range below 30ºC. On reducing the pH to 6.4, particle size decreased to ~50 nm in 0.75 mg/mL samples, and nanoparticle assembly was not observed at pH 6.2.

The formation of particles of two different sizes with increasing in temperature was also observed in (AG)60-(VH4)24 at concentrations above 0.5 mg/mL. This two-stage transition leading to the emergence of small and large particles in solution at 45°C, could be due to the formation of both weak micelles and larger aggregates during heating within the 30-45°C range. This can be attributed to the composition of ELPs: they are prone to forming secondary structures as they are polypeptides *via* the complete phase separation of the hydrophilic block from the solution over prolonged heating above their critical micelle temperature (CMT) **[91]**. CMT is the temperature above the ELP unimers self-assemble into micelles at a certain concentration.

### 4.3 ELP encapsulation and stability

The amount of DEX encapsulated by (AG)40-(VH4)24 is about 1.27 µg at 0.25 mg/mL ELP concentration. Although this could be perceived as a low dose, DEX amounts, as low as 0.1 µg administered via a single intracerebroventricular injection showed protection against HI injury in a neonatal rat model **[130]**. The main advantage of using a high molecular weight drug carrier is to increase the circulation half-life of a drug while lowering the therapeutic dosage **[103]**. The drug carrier also increases the solubility of a hydrophobic drug such as DEX. As a result, it allows repeated administration of the drug with less concerns about toxicity or side-effects in comparison to free drug administration.

Another way of increasing drug encapsulation in ELPs is by increasing the hydrophobicity of the guest amino acid and/or the length of the hydrophobic domain. The production of ELPs from genetic templates allows for convenient modification of the ELP molecular structure. Since encapsulation of DEX is primarily driven by hydrophobic interactions, increasing the hydrophobic nature of the ELP may in turn facilitate a greater quantity and more stable drug loading within the hydrophobic core of ELP nanoparticles.

The feasibility of readily packaging drugs into these ELP nanoparticles within a short span of time of <30 mins, facilitates drug delivery in an on-demand fashion and eliminates any concerns associated with short-term stability of the (AG)40-(VH4)24 particles.

### 4.4 Focal cooling

A promising treatment following brain injury in the newborn is to decrease brain temperature. However, there is a limited range of techniques for implementing focal head hypothermia in neonatal rodent models. Despite that rodents are more experimentally amenable and have easier husbandry than large animals and are used extensively to model developmental brain pathology, there have been only a few reports of focal head cooling in newborn rats. In one instance, ice water was conducted through a catheter inserted under the scalp ipsilateral to the ligated carotid artery for 2 hours, while simultaneously inducing hypoxia **[125]**. The core (rectal) and brain (dorsal hippocampus ipsilateral to the ligated artery) temperatures decreased rapidly within 15 min. of hypothermia and were approximately 32.2°C and 27.5°C, respectively, over the entire course of cooling **[125]**. Another approach was to secure to the rat head a metallic plate thermoregulator set at 30-32°C during 1.5 hours of hypoxia treatment and for an additional 1.5 hours of reperfusion **[126]**. The brain temperature was decreased to the desired range in 1 hour, while the core temperature was maintained at 35-36°C by a heating blanket and heat lamp **[126]**. Here, we propose a simple focal cooling device that involves a coil of cooling water fitted around the head of PD7 rats that can reduce brain temperature to 30-32°C. Unlike the previous rat studies, our method of focal brain cooling does not require surgical installation and was applied for a longer period of time, 24h. Moreover, cooling was induced after hypoxia treatment, rather than coinciding with hypoxia, to better simulate the clinical application of hypothermia after the hypoxic-ischemic incident. Among the multiple methods of focal cooling, the agreement is that decreasing the brain temperature attenuates the extent of brain damage.

We used whole-body cooling as a means to compare and validate our cooling device for use in experimental paradigms regarding neonatal brain injury. Indeed, the cooling device is capable of conferring neuroprotection similar to that of whole-body cooling. The parallel outcomes from the two cooling methods are consistent with clinical data **[127]** and are expected because either method is able to decrease the brain temperature. However, one clinical study reported better outcomes with whole-body than selective brain cooling when assessed by electroencephalography and magnetic resonance imaging **[128]**. In contrast, local hypothermia outperformed whole-body hypothermia in infants with severe cortical lesions **[129]**, and an explanation could be the local rate of temperature decrease at the wound. A cooling helmet can rapidly decrease the local temperature **[127]**, and the cerebral cortex is the closest brain structure in proximity to the heat exchange surface, whereas whole-body hypothermia may take a relatively longer time to decrease brain temperature because the body periphery and core are cooled prior to the brain. Although our model of hypoxic-ischemic encephalopathy produced cortical lesions, we observed no significant difference between focal or whole-body cooling for preventing cortical volume loss. A reason for the discrepancy between observations in infants and rats may be that the smaller size of the rat brain loses thermal energy relatively fast using either method.

Our approach to focal cooling has several advantages. A large number, up to an entire litter of eight pups, can be treated simultaneously for time-matched experiments, and the animals do not require invasive surgical manipulation or anaesthesia to receive cooling. It is not necessary to adjust the flowrate and temperature of the circulating water once these parameters are set at the start of hypothermia, thus eliminating the need for continuous temperature monitoring of the animals for feedback control. An additional advantage occurs as a result of the accessibility to the

animal model during cooling. Given that much research is now focussed on the use of medications **[63]** that may be supplemental to the benefits of hypothermia, our device allows for this provision

### 4.5 Biocompatibility of the diblock ELPs

Biocompatibility is an important criterion when selecting materials for biomedical applications. Presence of ELP signal in an organ does not always correspond with presence of drug, since drug release happens owing to pH and temperature changes, and ELP may still circulate. Understanding the dynamics of ELP as a function of organ/location within the system, on the other hand, is critical for determining the toxicity effects on that specific local area. Therefore, we analyzed the expression of protein biomarkers *in situ* to directly examine the tissue condition of the brain and major organs following ELP administration.

We screened for Casp3 cleavage to identify apoptotic cell death. Pro-apoptotic signals induce the irreversible proteolytic cleavage of pro-Casp3 to yield 17/19 kDa subunits of active Casp3 **[131]**. Activated Casp3 then cleaves a wide range of vital cellular components to degrade the cell into apoptotic bodies **[132]**. In my assessment, there was a basal level of Casp3 cleavage in liver tissue, but Casp3 fragments were not found in the brain, kidney, and heart. Nonetheless, the assessment of Casp3 cleavage at two days after ELP administration is expected to be within the timeframe of Casp3 activity should there be apoptosis occurring in the tissue.

The application of ELPs to the brain led me to consider neuroinflammation as a potential side-effect. Nanomaterial-induced injury to the brain is believed to stimulate astrocyte proliferation and activation, and astrocytes secrete pro-inflammatory factors that induce secondary damage after the initial injury **[134]**. Gfap is an intermediate filament of the astrocyte cytoskeleton important to maintaining the astrocyte morphology and is upregulated during reactive gliosis due to tissue damage **[134]**. For example, *in vivo* and *in vitro* studies demonstrated that carbon nanotubes and carbon black nanoparticles increased Gfap expression in mouse cortical astrocytes **[134]**. In contrast, our data indicate that Gfap expression in the brains of ELP-treated rats did not deviate from basal levels; thus, these specific ELPs are unlikely to provoke neuroinflammation.

Our data also indicates that ELP administration did not affect the basal expression of Iba1, a marker of macrophage activation, in the heart or liver. Notably, the Iba1 Western signal was absent in brain samples. An explanation is that, in the rat brain, Iba1 expression is specific to microglia and is absent in neurons, astrocytes, and meningeal fibroblasts **[135]**, and the PD7 microglia population is small **[136]**. The basal Iba1 level may be too low to be detected, but Iba1 upregulation is likely assessable because our lab identified microglia activation in a previous study conducted at a similar time point **[136]**. Thus, the fact that the ELPs did not increase Iba1 expression in the brain, heart, or liver, and in combination with the Gfap expression data, altogether suggest that the ELPs do not induce macrophage or microglia activation in the neonatal model.

### 4.6 ELP mediated DEX release in the brain

A single injection of ELP (AG)40-(VH4)24 loaded with ~1.25 µg DEX resulted in ~0.4 µg of DEX/g of brain tissue and thus validates the ability of ELP-DEX nanoparticles to reach the brain. The absence of a temperature trigger *via* hypothermia could be the reason behind the undetected DEX in the other systemic organs such as heart, liver, and kidney. A possible explanation for the small amount of DEX found in the brain of a normothermic rat, could be that the ELPs release DEX in response to the low pH in the ischemic microenvironment. Further probing into the pH changes at the site of damage, will verify this explanation.

### 4.7 Conclusion

ELPs are a unique class of tunable stimulus-responsive biopolymers, where the physicochemical properties have been characterized before, but only recently have ELPs gained increasing attention for *in vivo* applications. Therapeutic hypothermia is the only approved treatment against HI injury, despite its limited effectiveness in offering neuroprotection. Given that it is a well-established treatment for ameliorating the unfavorable neurodevelopmental outcomes, combining hypothermia with targeted drug delivery may help address this unmet clinical need by boosting its therapeutic potential by a large degree. It would also help circumvent challenges associated with systemic drug administration. This study that aims at utilizing the stimuli-responsiveness of the ELPs to trigger drug release by external cooling, is therefore significant in advancing the research involving the exploration of adjuvant therapies to hypothermia.

We have proposed a method of brain cooling for neonatal rats and demonstrated the effectiveness in reducing brain atrophy in an injury model. With only a limited number of methods readily available to test the effect of head cooling in animal models of newborn brain injury, our cooling device could serve as a convenient platform to study combinatorial treatments with hypothermia in neonatal rat models. Therefore, our cooling device can be a research tool in numerous preclinical analyses.

The ELPs we studied showed localization in the brain and did not cause observable adverse reactions in major organs of the neonatal rat within a short time period of administration. The study also illustrated the ability of the ELPs to form nanoparticles encapsulating DEX and release the drug in response to temperature and pH changes, under both *in vitro* and *in vivo* conditions. Next steps would be to inject the DEX-containing nanoparticles into the rat model and test the effectiveness of this treatment combined with hypothermia in reducing the extent of brain damage in comparison with hypothermia as a standalone treatment. Another important factor to establish would be the dose-response relationship of the ELP-mediated drug delivery in the rat model which would allude to the protective and potential toxic dosing levels in a clinical setting. In conclusion, our work has opened a new avenue for expanding the biomedical applications of the ELPs into the realm of neonatal brain injury and has also provided a promising complimentary therapy to augment the effect of hypothermia. The ELP-based delivery vehicle can then be used as a tool, in future pharmacological pre-clinical studies for drug screening. Bench to bedside translation of this treatment also holds promise to improve the survival and quality of life in babies that experience HI insult.

# Chapter 5:

# Future directions

## 5.1 Prospective Studies

### 5.1.1 Testing the combinatorial effect of ELP-DEX and hypothermia treatment

Our study showed that ELPs respond to focal cooling applied to the brain area and/pH changes caused due to local acidosis to release DEX, that was detected in the brain tissue. Since our goal is to augment the benefits of hypothermia, future studies will investigate if the combination treatment elicits better neuroprotection than hypothermia-only and DEX-only treatments in the rat model. The next step would also involve determining the appropriate dosing regimen of DEX *via* ELP-mediated delivery and compare it with free DEX administration.

### 5.1.2 Behavioral testing and biomarker expression analysis

The efficacy of ELP-DEX treatment will primarily be investigated at the anatomical and molecular level by measuring brain infarct volumes in healthy vs damaged hemisphere and quantifying the expressions of neuroinflammatory (e.g., Gfap, Iba1) and apoptotic markers (e.g., Casp3, Bcl, Bax).

Behavioral analysis is a determinant of long-term neurodevelopmental outcomes and is crucial for clinical translatability from *in vivo* studies. Therefore, future work in the project would also involve the assessment of behavioral and cognitive phenotypes such as spatial learning, memory, motor functions, sensory processing, sensory-motor reflexes, attention, and emotional states (anxiety) **[2,137]**.

### 5.1.3 Incorporating other drugs

DEX was chosen for this study owing to the ability to confer protection against moderate to severe HI injury in neonatal animal models **[130]**. Since ELPs possess a wide variety of drug delivery applications, other pharmacological agents that are under investigation for treating neonatal HI injury can be studied by using ELPs as the drug carrier. For instance, MK-801, an NMDA receptor antagonist that was extensively studied for use in treating HI injury to inhibit excitotoxicity **[138]**. However, since NMDA receptors are ubiquitous in the brain and glutamate is an important excitatory neurotransmitter for normal brain development, non-specific distribution of the drug could cause undesirable side effects **[138]**. Localizing the drug by targeted release via ELPs could be a potential solution.

### 5.1.4 Increasing the specificity of ELP targeting

Given that ELPs have tunable properties that can be modified by genetic engineering, distinct targeting ligands can be appended to ELPs for targeted drug delivery systems. Several studies have worked on improving the tumor targeting capabilities of ELPs by tagging ELPs with tumor specific cell surface receptors and cell penetrating peptides **[103,112]**. Similarly, release of drug from the ELP can be made to specifically target the tissue microenvironment at the site of damage by fusing ELPs with appropriate ligand or receptor peptide motifs, where the peptide tags can be identified via in vivo phage display screening.

### 5.1.5 Determining ELP kinetics *in vivo*

It is necessary to consider the long-term aspects of ELP biocompatibility, for example the effects of repeated ELP administration on cellular uptake, distribution, accumulation and elimination within the system. ELP length, guest amino acid composition, and phase transition are key parameters for ELP functionality, but their effects on biocompatibility, and mechanisms of clearance are not well understood. Future studies could work on understanding how ELPs interact in biological milieus since it is paramount for developing safe biomedical applications, especially when translating to humans.

## 5.2 Limitations

### 5.2.1 Animal model and age

PD7 Long-Evans rats have been chosen for this study since the PD7 rodent brain is a conventional model of the human brain at 36-40 weeks of gestation **[120]**. However, a limitation with using animals at this age would be the choice of administration route. With intravenous and subcutaneous routes, the drug becomes readily available and by-passes first pass metabolism. However, since these animals are quite young, their arteries and veins are small and difficult to utilize, thereby making intravenous administration a challenging one. Similarly, intra-arterial injection directly *via* the carotid artery, may increase the risk of mortality. Subcutaneous route would take a longer time to reach the brain due to slower absorption **[139]**. While intracerebroventricular gives direct access to the brain, it is a highly invasive and time-consuming procedure **[139]**. Intraperitoneal injections is relatively the best suited option, but it may result in increased biodistribution of the ELP nanoparticles. This can, however, be circumvented by multiple dosing. Keeping this in mind,

method of administration and dosing are two important factors that need to be optimized clinical translation.

Rice-Vannucci model of HI injury is used in this project because a) the model has been well characterized and is reflective of the anatomical and metabolic changes that occurs in humans post HI damage **[2]** b) It is one of the most commonly employed models to study HI and neonatal neuroprotection **[2]** c) Neurobehavioral outcomes following HI and hypothermia treatment have been thoroughly studied **[2]** d) Since it involves unilateral ligation, the contralateral hemisphere within the experimental brain could serve as a control **[2]**. Despite these advantages, the major setback with using this model is the high degree of variability between animals in terms of size and severity of the brain damage achieved, thus making it challenging to compare results between experiments/experimenters and achieve statistical significance with a small number of animals.

### 5.2.2 Cooling device

There is a limitation to the proposed cooling device, as cooling the entire head also produces mild systemic hypothermia. In an earlier study, head cooling reduced the core temperature to 32.2°C **[125].** Systemic cooling occurs presumably as a by-product because blood circulation equilibrates thermal energy throughout the body, but our cooling device maintains a core temperature around 3.2°C higher than that of the brain.

Although selective head cooling is effective in ameliorating the damage, it could lead to a temperature gradient from brain surface to deepest areas as basal ganglia and brain stem; that

gradient reaches 7 ºC at depths of 2 cm in piglets **[140]**. The temperature gradient could reduce the efficacy of the targeted release mechanism of the ELPs, especially the ones that are solely temperature dependent. This is because if the injury is in deeper areas of the brain, and insufficient cooling in this area due to the gradient in bigger animals and humans, may not trigger the disassembly of a temperature sensitive ELP for drug release. Using ELPs that can respond to more than one external cue specific to the HI brain microenvironment like the pH sensitive ELPs used in our study, may help overcome this limitation.

**Bibliography**


1. Novak CM, Ozen M, Burd I. Perinatal brain injury: mechanisms, prevention, and outcomes. Clinics in perinatology. 2018 Jun 1;45(2):357-75.
2. Millar LJ, Shi L, Hoerder-Suabedissen A, Molnár Z. Neonatal hypoxia ischaemia: mechanisms, models, and therapeutic challenges. Frontiers in cellular neuroscience. 2017 May 8;11:78.
3. Hack M, Breslau N, Aram D, Weissman B, Klein N, Borawski-Clark E. The effect of very low birth weight and social risk on neurocognitive abilities at school age. Journal of Developmental and Behavioral Pediatrics. 1992 Dec.
4. Vannucci SJ, Hagberg H. Hypoxia–ischemia in the immature brain. Journal of Experimental Biology. 2004 Aug 15;207(18):3149-54.
5. Dixon BJ, Reis C, Ho WM, Tang J, Zhang JH. Neuroprotective strategies after neonatal hypoxic-ischemic encephalopathy. International journal of molecular sciences. 2015 Sep;16(9):22368-401.
6. Prempunpong C, Chalak LF, Garfinkle J, Shah B, Kalra V, Rollins N, Boyle R, Nguyen KA, Mir I, Pappas A, Montaldo P. Prospective research on infants with mild encephalopathy: the PRIME study. Journal of Perinatology. 2018 Jan;38(1):80-5.
7. Conway JM, Walsh BH, Boylan GB, Murray DM. Mild hypoxic ischaemic encephalopathy and long term neurodevelopmental outcome-A systematic review. Early human development. 2018 May 1;120:80-7.
8. Logitharajah P, Rutherford MA, Cowan FM. Hypoxic-ischemic encephalopathy in preterm infants: antecedent factors, brain imaging, and outcome. Pediatric research. 2009 Aug;66(2):222-9.
9. Kurinczuk JJ, White-Koning M, Badawi N. Epidemiology of neonatal encephalopathy and hypoxic–ischaemic encephalopathy. Early human development. 2010 Jun 1;86(6):329-38.
10. Douglas-Escobar M, Weiss MD. Hypoxic-ischemic encephalopathy: a review for the clinician. JAMA pediatrics. 2015 Apr 1;169(4):397-403.
11. Sweeney MI, Waiz W, Yager JY, Juurlink B. Cellular mechanisms involved in brain ischemia. Canadian journal of physiology and pharmacology. 1995 Nov 1;73(11):1525-35.
12. Askalan R, Salweski R, Tuor UI, Hutchison J, Hawkins C. X-linked inhibitor of apoptosis protein expression after ischemic injury in the human and rat developing brain. Pediatric research. 2009 Jan;65(1):21-6.
13. Askalan R, Wang C, Shi H, Armstrong E, Yager JY. The effect of postischemic hypothermia on apoptotic cell death in the neonatal rat brain. Developmental neuroscience. 2011;33(3-4):320-9.
14. Zhang F, Wang S, Luo Y, Ji X, Nemoto EM, Chen J. When hypothermia meets hypotension and hyperglycemia: the diverse effects of adenosine 5′-monophosphate on cerebral ischemia in rats. Journal of Cerebral Blood Flow & Metabolism. 2009 May;29(5):1022-34.

**15.** Wassink G, Davidson JO, Lear CA, Juul SE, Northington F, Bennet L, Gunn AJ. A working model for hypothermic neuroprotection. The Journal of physiology. 2018 Dec;596(23):5641-54.
16. Vannucci RC. Experimental biology of cerebral hypoxia-ischemia: relation to perinatal brain damage. Pediatric research. 1990 Apr;27(4):317-26.
17. Davies A, Wassink G, Bennet L, Gunn AJ, Davidson JO. Can we further optimize therapeutic hypothermia for hypoxic-ischemic encephalopathy?. Neural regeneration research. 2019 Oct;14(10):1678.
18. Choi DW, Rothman SM. The role of glutamate neurotoxicity in hypoxic-ischemic neuronal death. Annual review of neuroscience. 1990 Mar;13(1):171-82.
19. Chan PH. Reactive oxygen radicals in signaling and damage in the ischemic brain. Journal of Cerebral Blood Flow & Metabolism. 2001 Jan;21(1):2-14.
20. Nair J, Kumar VH. Current and emerging therapies in the management of hypoxic-ischemic encephalopathy in neonates. Childgreren. 2018 Jul;5(7):99.
21. Allen KA, Brandon DH. Hypoxic-ischemic encephalopathy: pathophysiology and experimental treatments. Newborn and Infant Nursing Reviews. 2011 Sep 1;11(3):125-33.
22. Felderhoff-Müser U. Is There More than Cooling to Protect the Brain?. InInnovations and Frontiers in Neonatology 2020 (Vol. 22, pp. 143-158). Karger Publishers.
23. Lafemina MJ, Sheldon RA, Ferriero DM. Acute hypoxia-ischemia results in hydrogen peroxide accumulation in neonatal but not adult mouse brain. Pediatric research. 2006 May;59(5):680.
24. Ikonomidou C, Kaindl AM. Neuronal death and oxidative stress in the developing brain. Antioxidants & redox signaling. 2011 Apr 15;14(8):1535-50.
25. Zubrow AB, Delivoria-Papadopoulos M, Ashraf QM, Fritz KI, Mishra OP. Nitric oxide-mediated Ca2+/calmodulin-dependent protein kinase IV activity during hypoxia in neuronal nuclei from newborn piglets. Neuroscience letters. 2002 Dec 19;335(1):5-8.
26. Greco P, Nencini G, Piva I, Scioscia M, Volta CA, Spadaro S, Neri M, Bonaccorsi G, Greco F, Cocco I, Sorrentino F. Pathophysiology of hypoxic–ischemic encephalopathy: a review of the past and a view on the future. Acta Neurologica Belgica. 2020 Feb 28:1-2.
27. Lu Y, Tucker D, Dong Y, Zhao N, Zhuo X, Zhang Q. Role of mitochondria in neonatal hypoxic-ischemic brain injury. Journal of neuroscience and rehabilitation. 2015;2(1):1.
28. Erecińska M, Silver IA. Ions and energy in mammalian brain. Progress in neurobiology. 1994 May 1;43(1):37-71.
29. Gilland E, Puka-Sundvall M, Hillered L, Hagberg H. Mitochondrial function and energy metabolism after hypoxia—ischemia in the immature rat brain: involvement of NMDA-receptors. Journal of Cerebral Blood Flow & Metabolism. 1998 Mar;18(3):297-304.
30. Edwards AB, Anderton RS, Knuckey NW, Meloni BP. Perinatal hypoxic-ischemic encephalopathy and neuroprotective peptide therapies: A case for cationic arginine-rich peptides (CARPs). Brain sciences. 2018 Aug;8(8):147.

31. Johnston MV. Excitotoxicity in perinatal brain injury. Brain pathology. 2005 Jul;15(3):234-40.
32. Olney JW, Price MT, Samson L, Labruyere J. The role of specific ions in glutamate neurotoxicity. Neuroscience letters. 1986 Mar 28;65(1):65-71.
33. Choi DW. Excitotoxic cell death. Journal of neurobiology. 1992 Nov;23(9):1261-76.
34. Stout AK, Raphael HM, Kanterewicz BI, Klann E, Reynolds IJ. Glutamate-induced neuron death requires mitochondrial calcium uptake. Nature neuroscience. 1998 Sep;1(5):366-73.
35. Johnston MV, Trescher WH, Ishida A, Nakajima W. Neurobiology of hypoxic-ischemic injury in the developing brain. Pediatric research. 2001 Jun;49(6):735-41.
36. Iadecola C, Anrather J. The immunology of stroke: from mechanisms to translation. Nature medicine. 2011 Jul;17(7):796.
37. Algra SO, Groeneveld KM, Schadenberg AW, Haas F, Evens FC, Meerding J, Koenderman L, Jansen NJ, Prakken BJ. Cerebral ischemia initiates an immediate innate immune response in neonates during cardiac surgery. Journal of neuroinflammation. 2013 Dec;10(1):796.
38. Ziemka-Nalecz M, Jaworska J, Zalewska T. Insights into the neuroinflammatory responses after neonatal hypoxia-ischemia. Journal of Neuropatholgy & Experimental Neurology. 2017 Aug 1;76(8):644-54.
39. Liu F, Mccullough LD. Inflammatory responses in hypoxic-ischemic encephalopathy. Acta Pharmacologica Sinica. 2013 Sep;34(9):1121-30.
40. Baggiolini MJ. Chemokines in pathology and medicine. Journal of internal medicine. 2001 Aug 19;250(2):91-104.
41. Vezzani A, Aronica E, Mazarati A, Pittman QJ. Epilepsy and brain inflammation. Experimental neurology. 2013 Jun 1;244:11-21.
42. Youn Y, Sung IK, Lee IG. The role of cytokines in seizures: interleukin (IL)-1β, IL-1Ra, IL-8, and IL-10. Korean journal of pediatrics. 2013 Jul;56(7):271.
43. Bernardi P, Krauskopf A, Basso E, Petronilli V, Blalchy-Dyson E, Di Lisa F, Forte MA. The mitochondrial permeability transition from in vitro artifact to disease target. The FEBS journal. 2006 May 1;273(10):2077-99.
44. Thornton C, Rousset CI, Kichev A, Miyakuni Y, Vontell R, Baburamani AA, Fleiss B, Gressens P, Hagberg H. Molecular mechanisms of neonatal brain injury. Neurology research international. 2012;2012.
45. Juurlink BH, Hertz L, Yager JY. Astrocyte maturation and susceptibility to ischaemia or substrate deprivation. Neuroreport. 1992 Dec;3(12):1135-7.
46. Ek CJ, D'angelo B, Baburamani AA, Lehner C, Leverin AL, Smith PL, Nilsson H, Svedin P, Hagberg H, Mallard C. Brain barrier properties and cerebral blood flow in neonatal mice exposed to cerebral hypoxia-ischemia. Journal of Cerebral Blood Flow & Metabolism. 2015 May;35(5):818-27.
47. Kumar A, Mittal R, Khanna HD, Basu S. Free radical injury and blood-brain barrier permeability in hypoxic-ischemic encephalopathy. Pediatrics. 2008 Sep 1;122(3):e722-7.

48. Lee WL, Michael-Titus AT, Shah DK. Hypoxic-ischaemic encephalopathy and the blood-brain barrier in neonates. Developmental neuroscience. 2017;39(1-4):49-58.
49. Disdier C, Stonestreet BS. Hypoxic-ischemic-related cerebrovascular changes and potential therapeutic strategies in the neonatal brain. Journal of neuroscience research. 2020 Jul;98(7):1468-84.
50. Edwards AD, Brocklehurst P, Gunn AJ, Halliday H, Juszczak E, Levene M, Strohm B, Thoresen M, Whitelaw A, Azzopardi D. Neurological outcomes at 18 months of age after moderate hypothermia for perinatal hypoxic ischaemic encephalopathy: synthesis and meta-analysis of trial data. Bmj. 2010 Feb 9;340:c363.
51. Higgins RD, Raju T, Edwards AD, Azzopardi DV, Bose CL, Clark RH, Ferriero DM, Guillet R, Gunn AJ, Hagberg H, Hirtz D. Hypothermia and other treatment options for neonatal encephalopathy: an executive summary of the Eunice Kennedy Shriver NICHD workshop. The Journal of pediatrics. 2011 Nov 1;159(5):851-8.
52. Cornette L. Therapeutic hypothermia in neonatal asphyxia. Facts, views & vision in ObGyn. 2012;4(2):133.
53. Tagin MA, Woolcott CG, Vincer MJ, Whyte RK, Stinson DA. Hypothermia for neonatal hypoxic-ischemic encephalopathy: an updated systematic review and meta-analysis. Archives of pediatrics & adolescent medicine. 2012 Jun 1;166(6):558-66.
54. Jacobs SE, Berg M, Hunt R, Tarnow-Mordi WO, Inder TE, Davis PG. Cooling for newborns with hypoxic ischaemic encephalopathy. Cochrane database of systematic reviews. 2013(1).
55. Cho KH, Davidson JO, Dean JM, Bennet L, Gunn AJ. Cooling and immunomodulation for treating hypoxic-ischemic brain injury. Pediatrics International. 2020 Jul;62(7):770-8.
56. Wassink G, Gunn ER, Drury PP, Bennet L, Gunn AJ. The mechanisms and treatment of asphyxial encephalopathy. Frontiers in neuroscience. 2014 Feb 27;8:40.
57. Gunn AJ, Hagberg H, Hirtz D. Hypothermia and other treatment options for neonatal encephalopathy: an executive summary of the Eunice Kennedy Shriver NICHD workshop. The Journal of pediatrics. 2011 Nov 1;159(5):851-8.
58. Wassink G, Davidson JO, Dhillon SK, Zhou K, Bennet L, Thoresen M, Gunn AJ. Therapeutic hypothermia in neonatal hypoxic-ischemic encephalopathy. Current neurology and neuroscience reports. 2019 Jan 1;19(1):2.
59. Liu G, Li ZG, Gao JS. Hypothermia in neonatal hypoxic-ischemic encephalopathy (HIE). Eur Rev Med Pharmacol Sci. 2017 Oct;21(4 Suppl):50-3.
60. Jackson TC, Kochanek PM (2019) A New Vision for Therapeutic Hypothermia in the Era of Targeted Temperature Management: A Speculative Synthesis. *Ther Hypothermia Temp Manag* 9:13–47.
61. Trescher WH, Ishiwa S, Johnston MV. Brief post-hypoxic-ischemic hypothermia markedly delays neonatal brain injury. Brain and Development. 1997 Jul 1;19(5):326-38.
62. Yager JY, Armstrong E, Osmond L. The duration of post-ischemic hypothermia as a neuroprotectant. Pediatric Research. 1999 Apr;45(7):349-.

63. Narayanamurthy R, Yang JL, Yager JY, Unsworth LD. Drug delivery platforms for neonatal brain injury. Journal of Controlled Release. 2021 Feb 10;330:765-87.
64. Ren JM, Finklestein SP (2005) Growth factor treatment of stroke. Curr Drug Targets CNS Neurol Disord 4:121-125.
65. Xiong T, Qu Y, Mu D, Ferriero D. Erythropoietin for neonatal brain injury: opportunity and challenge. International Journal of Developmental Neuroscience. 2011 Oct 1;29(6):583-91.
66. Chattopadhyay A, Choudhury TD, Bandyopadhyay D, Datta AG. Protective effect of erythropoietin on the oxidative damage of erythrocyte membrane by hydroxyl radical. Biochemical pharmacology. 2000 Feb 15;59(4):419-25.
67. Juul SE, Pet GC. Erythropoietin and neonatal neuroprotection. Clinics in perinatology. 2015 Sep 1;42(3):469-81.
68. Chau M, Chen D, Wei L (2011) Erythropoietin attenuates inflammatory factors and cell death in neonatal rats with intracerebral hemorrhage. Acta Neurochir Suppl 111:299-305.
69. Ehrenreich H, Weissenborn K, Prange H, Schneider D, Weimar C, Wartenberg K, Schellinger PD, Bohn M, Becker H, Wegrzyn M, Jähnig P, Herrmann M, Knauth M, Bähr M, Heide W, Wagner A, Schwab S, Reichmann H, Schwendemann G, Dengler R, Kastrup A, Bartels C (2009) Recombinant human erythropoietin in the treatment of acute ischemic stroke. Stroke 40:e647-e656.
70. Juul SE, Ferriero DM. Pharmacologic neuroprotective strategies in neonatal brain injury. Clinics in perinatology. 2014 Mar 1;41(1):119-31.
71. Ikonomidou C, Turski L. Why did NMDA receptor antagonists fail clinical trials for stroke and traumatic brain injury?. The Lancet Neurology. 2002 Oct 1;1(6):383-6.
72. Costantine MM, Drever N. Antenatal exposure to magnesium sulfate and neuroprotection in preterm infants. Obstetrics and Gynecology Clinics. 2011 Jun 1;38(2):351-66.
73. Qin X, Cheng J, Zhong Y, Mahgoub OK, Akter F, Fan Y, Aldughaim M, Xie Q, Qin L, Gu L, Jian Z, Xiong X, Liu R (2019) Mechanism and Treatment Related to Oxidative Stress in Neonatal Hypoxic-Ischemic Encephalopathy. Front Mol Neurosci 12:88.
74. McCord JM (1985) Oxygen-derived free radicals in postischemic tissue injury. N Engl J Med 312:159-163.
75. Thoresen M, Hobbs CE, Wood T, Chakkarapani E, Dingley J. Cooling Combined with Immediate or Delayed Xenon Inhalation Provides Equivalent Long-Term Neuroprotection after Neonatal Hypoxia—Ischemia. Journal of Cerebral Blood Flow & Metabolism. 2009 Apr;29(4):707-14.
76. Barks JD, Liu YQ, Shangguan Y, Silverstein FS. Phenobarbital augments hypothermic neuroprotection. Pediatric research. 2010 May;67(5):532-7.
77. Hendaus MA, Jomha FA, Alhammadi AH. Melatonin in the management of perinatal hypoxic-ischemic encephalopathy: light at the end of the tunnel?. Neuropsychiatric disease and treatment. 2016;12:2473.

78. Concepcion KR, Zhang L. Corticosteroids and perinatal hypoxic-ischemic brain injury. Drug discovery today. 2018 Oct 1;23(10):1718-32.
79. Felszeghy K, Banisadr G, Rostène W, Nyakas C, Haour F. Dexamethasone downregulates chemokine receptor CXCR4 and exerts neuroprotection against hypoxia/ischemia-induced brain injury in neonatal rats. Neuroimmunomodulation. 2004;11(6):404-13.
80. Feng Y, Rhodes PG, Bhatt AJ. Dexamethasone pre-treatment protects brain against hypoxic-ischemic injury partially through up-regulation of vascular endothelial growth factor A in neonatal rats. Neuroscience. 2011 Apr 14;179:223-32.
81. Feng Y, Rhodes PG, Bhatt AJ. Dexamethasone pre-treatment protects brain against hypoxic-ischemic injury partially through up-regulation of vascular endothelial growth factor A in neonatal rats. Neuroscience. 2011 Apr 14;179:223-32.
82. Ikeda T, Mishima K, Yoshikawa T, Iwasaki K, Fujiwara M, Xia YX, Ikenoue T. Dexamethasone prevents long-lasting learning impairment following neonatal hypoxic–ischemic brain insult in rats. Behavioural brain research. 2002 Oct 17;136(1):161-70.
83. Sandercock PA, Soane T. Corticosteroids for acute ischaemic stroke. Cochrane database of systematic reviews. 2011(9).
84. Chang KH, Yeh CM, Yeh CY, Huang CC, Hsu KS. Neonatal dexamethasone treatment exacerbates hypoxic-ischemic brain injury. Molecular Brain. 2013 Dec 1;6(1):18.
85. Alshememry AK, El-Tokhy SS, Unsworth LD. Using properties of tumor microenvironments for controlling local, on-demand delivery from biopolymer-based nanocarriers. Current pharmaceutical design. 2017 Oct 1;23(35):5358-91.
86. Callahan DJ, Liu W, Li X, Dreher MR, Hassouneh W, Kim M, Marszalek P, Chilkoti A. Triple stimulus-responsive polypeptide nanoparticles that enhance intratumoral spatial distribution. Nano letters. 2012 Apr 11;12(4):2165-70.
87. MacKay JA, Callahan DJ, FitzGerald KN, Chilkoti A. Quantitative model of the phase behavior of recombinant pH-responsive elastin-like polypeptides. Biomacromolecules. 2010 Nov 8;11(11):2873-9.
88. Bahniuk MS, Alshememry AK, Elgersma SV, Unsworth LD. Self-assembly/disassembly hysteresis of nanoparticles composed of marginally soluble, short elastin-like polypeptides. Journal of nanobiotechnology. 2018 Dec 1;16(1):15.
89. Urry DW, Luan CH, Parker TM, Gowda DC, Prasad KU, Reid MC, Safavy A. Temperature of polypeptide inverse temperature transition depends on mean residue hydrophobicity. Journal of the American Chemical Society. 1991 May;113(11):4346-8.
90. Fletcher EE, Yan D, Kosiba AA, Zhou Y, Shi H. Biotechnological applications of elastin-like polypeptides and the inverse transition cycle in the pharmaceutical industry. Protein expression and purification. 2019 Jan 1;153:114-20.
91. Hassouneh W, Zhulina EB, Chilkoti A, Rubinstein M. Elastin-like polypeptide diblock copolymers self-assemble into weak micelles. Macromolecules. 2015 Jun 23;48(12):4183-95.

92. MacEwan SR, Chilkoti A. Applications of elastin-like polypeptides in drug delivery. Journal of Controlled Release. 2014 Sep 28;190:314-30.
93. Urry DW, Gowda DC, Parker TM, Luan CH, Reid MC, Harris CM, et al. Hydrophobicity scale for proteins based on inverse temperature transitions. Biopolymers. 1992;32:1243-50.
94. Widder K, MacEwan SR, Garanger E, Núñez V, Lecommandoux S, Chilkoti A, Hinderberger D. Characterisation of hydration and nanophase separation during the temperature response in hydrophobic/hydrophilic elastin-like polypeptide (ELP) diblock copolymers. Soft Matter. 2017;13(9):1816-22.
95. Li NK, Quiroz FG, Hall CK, Chilkoti A, Yingling YG. Molecular description of the LCST behavior of an elastin-like polypeptide. Biomacromolecules. 2014 Oct 13;15(10):3522-30.
96. Muiznieks LD, Keeley FW. Proline periodicity modulates the self-assembly properties of elastin-like polypeptides. Journal of Biological Chemistry. 2010 Dec 17;285(51):39779-89.
97. Urry DW. Physical chemistry of biological free energy transduction as demonstrated by elastic protein-based polymers. The Journal of Physical Chemistry B. 1997 Dec 18;101(51):11007-28.
98. Kammer HW, Inoue T, Ougizawa T. Upper and lower critical solution temperature behaviour in polymer blends and its thermodynamic interpretation. Polymer. 1989 May 1;30(5):888-92.
99. Thomas EL. The ABCs of self-assembly. Science. 1999 Nov 12;286(5443):1307-.
100. Riess G. Micellization of block copolymers. Progress in polymer science. 2003 Jul 1;28(7):1107-70.
101. Bahniuk MS, Alshememry AK, Unsworth LD. High-yield recombinant expression and purification of marginally soluble, short elastin-like polypeptides. BioTechniques. 2016 Dec;61(6):297-304.
102. Meyer DE, Chilkoti A. Genetically encoded synthesis of protein-based polymers with precisely specified molecular weight and sequence by recursive directional ligation: examples from the elastin-like polypeptide system. Biomacromolecules. 2002 Mar 11;3(2):357-67.
103. Varanko AK, Su JC, Chilkoti A. Elastin-like polypeptides for biomedical applications. Annual Review of Biomedical Engineering. 2020 Jun 4;22:343-69.
104. Saxena R, Nanjan MJ. Elastin-like polypeptides and their applications in anticancer drug delivery systems: a review. Drug delivery. 2015 Feb 17;22(2):156-67.
105. Nettles DL, Chilkoti A, Setton LA. Applications of elastin-like polypeptides in tissue engineering. Advanced drug delivery reviews. 2010 Dec 30;62(15):1479-85.
106. Betre H, Chilkoti A, Setton LA. A two-step chondrocyte recovery system based on thermally sensitive elastin-like polypeptide scaffolds for cartilage tissue engineering. InProceedings of the Second Joint 24th Annual Conference and the Annual Fall Meeting of

the Biomedical Engineering Society][Engineering in Medicine and Biology 2002 Oct 23 (Vol. 1, pp. 829-830). IEEE.
107. Trabbic-Carlson K, Liu L, Kim B, Chilkoti A. Expression and purification of recombinant proteins from Escherichia coli: Comparison of an elastin-like polypeptide fusion with an oligohistidine fusion. Protein Science. 2004 Dec;13(12):3274-84.
108. Kowalczyk T, Hnatuszko-Konka K, Gerszberg A, Kononowicz AK. Elastin-like polypeptides as a promising family of genetically-engineered protein based polymers. World Journal of Microbiology and Biotechnology. 2014 Aug;30(8):2141-52.
109. Hassouneh W, Christensen T, Chilkoti A. Elastin-like polypeptides as a purification tag for recombinant proteins. Current protocols in protein science. 2010 Aug;61(1):6-11.
110. Yeboah A, Cohen RI, Rabolli C, Yarmush ML, Berthiaume F. Elastin-like polypeptides: A strategic fusion partner for biologics. Biotechnology and bioengineering. 2016 Aug;113(8):1617-27.
111. Andrew Mackay J, Chilkoti A. Temperature sensitive peptides: engineering hyperthermia-directed therapeutics. International Journal of Hyperthermia. 2008 Jan 1;24(6):483-95.
112. McDaniel JR, Callahan DJ, Chilkoti A. Drug delivery to solid tumors by elastin-like polypeptides. Advanced drug delivery reviews. 2010 Dec 30;62(15):1456-67.
113. Liu W, Dreher MR, Furgeson DY, Peixoto KV, Yuan H, Zalutsky MR, Chilkoti A. Tumor accumulation, degradation and pharmacokinetics of elastin-like polypeptides in nude mice. Journal of controlled release. 2006 Nov 28;116(2):170-8.
114. Massodi I, Bidwell III GL, Raucher D. Evaluation of cell penetrating peptides fused to elastin-like polypeptide for drug delivery. Journal of controlled release. 2005 Nov 28;108(2-3):396-408.
115. Amruthwar SS, Janorkar AV. Preparation and characterization of elastin-like polypeptide scaffolds for local delivery of antibiotics and proteins. Journal of Materials Science: Materials in Medicine. 2012 Dec;23(12):2903-12.
116. Adams Jr SB, Shamji MF, Nettles DL, Hwang P, Setton LA. Sustained release of antibiotics from injectable and thermally responsive polypeptide depots. Journal of Biomedical Materials Research Part B: Applied Biomaterials. 2009 Jul;90(1):67-74.
117. Cho S, Dong S, Parent KN, Chen M. Immune-tolerant elastin-like polypeptides (iTEPs) and their application as CTL vaccine carriers. Journal of drug targeting. 2016 Apr 20;24(4):328-39.
118. Smits FC, Buddingh BC, van Eldijk MB, van Hest JC. Elastin-like polypeptide based nanoparticles: Design rationale toward nanomedicine. Macromolecular bioscience. 2015 Jan;15(1):36-51.
119. Rodríguez-Cabello JC, Arias FJ, Rodrigo MA, Girotti A. Elastin-like polypeptides in drug delivery. Advanced drug delivery reviews. 2016 Feb 1;97:85-100.
120. Yager JY, Ashwal S. Animal models of perinatal hypoxic-ischemic brain damage. Pediatric neurology. 2009 Mar 1;40(3):156-67.

121. Grippa E, Santini L, Castellano G, Gatto MT, Leone MG, Saso L. Simultaneous determination of hydrocortisone, dexamethasone, indomethacin, phenylbutazone and oxyphenbutazone in equine serum by high-performance liquid chromatography. Journal of Chromatography B: Biomedical Sciences and Applications. 2000 Jan 28;738(1):17-25.
122. Athina Samara, George T Tsangaris (2011) Brain asymmetry: both sides of the story
123. Joseph A, Wood T, Chen CC, Corry K, Snyder JM, Juul SE, Parikh P, Nance E. Curcumin-loaded polymeric nanoparticles for neuroprotection in neonatal rats with hypoxic-ischemic encephalopathy. Nano research. 2018 Oct;11(10):5670-88.
124. Gubits RM, Burke RE, Casey-McIntosh G, Bandele A, Munell F (1993) Immediate early gene induction after neonatal hypoxia-ischemia
125. Towfighi J, Housman C, Heitjan DF, Vannucci RC, Yager JY (1994) The effect of focal cerebral cooling on perinatal hypoxic-ischemic brain damage. *Acta Neuropathologica* 87:598–604.
126. Hashimoto T, Yonetani M, Nakamura H (2004) Selective brain hypothermia protects against hypoxic-ischemic injury in newborn rats by reducing hydroxyl radical production. *Kobe J Med Sci* 49:83–92.
127. Sun YJ, Zhang ZY, Fan B, Li GY (2019) Neuroprotection by Therapeutic Hypothermia. *Front Neurosci* 13:586.
128. Goenka A, Yozawitz E, Gomes WA, Nafday SM (2020) Selective Head versus Whole Body Cooling Treatment of Hypoxic-Ischemic Encephalopathy: Comparison of Electroencephalogram and Magnetic Resonance Imaging Findings. Am J Perinatol 37:1264–1270.
129. Rutherford MA, Azzopardi D, Whitelaw A, Cowan F, Renowden S, Edwards AD, Thoresen M (2005) Mild hypothermia and the distribution of cerebral lesions in neonates with hypoxic-ischemic encephalopathy. *Pediatrics* 116:1001–1006.
130. Harding B, Conception K, Li Y, Zhang L. Glucocorticoids protect neonatal rat brain in model of hypoxic-ischemic encephalopathy (HIE). International journal of molecular sciences. 2016 Dec 22;18(1):17.
131. Ferreira KS, Kreutz C, Macnelly S, Neubert K, Haber A, Bogyo M, Timmer J, Borner C. (2012) Caspase-3 feeds back on caspase-8, Bid and XIAP in type I Fas signaling in primary mouse hepatocytes.
132. Beroske L, Van den Wyngaert T, Stroobants S, Van der Veken P, Elvas F. (2021) Molecular Imaging of Apoptosis: The Case of Caspase-3 Radiotracers.
133. X Wang, J O Karlsson, C Zhu, B A Bahr, H Hagberg, K Blomgren (2001) Caspase-3 Activation after Neonatal Rat Cerebral Hypoxia-Ischemia
134. Danni Dai, Longwen He, Yuming Chen, Chao Zhang (2021) Astrocyte responses to nanomaterials: Functional changes, pathological changes and potential applications
135. Daisuke Ito, MD; Kortaro Tanaka, MD; Shigeaki Suzuki, MD; Tomohisa Dembo, MD; Yasuo Fukuuchi, MD (2001) Enhanced Expression of Iba1, Ionized Calcium-Binding Adapter Molecule 1, After Transient Focal Cerebral Ischemia In Rat Brain

136. Lei Lu, Edward A Armstrong, Jerome Y Yager, Larry D Unsworth (2019) Sustained Release of Dexamethasone from Sulfobutyl Ether
137. Nguyen AT, Armstrong EA, Yager JY. Neurodevelopmental reflex testing in neonatal rat pups. JoVE (Journal of Visualized Experiments). 2017 Apr 24(122):e55261.
138. Zhang X, Peng K, Zhang X. The function of the NMDA receptor in hypoxic-ischemic encephalopathy. Frontiers in Neuroscience. 2020:998.
139. Turner PV, Brabb T, Pekow C, Vasbinder MA. Administration of substances to laboratory animals: routes of administration and factors to consider. Journal of the American Association for Laboratory Animal Science. 2011 Sep 15;50(5):600-13.
140. Laptook AR, Shalak L, Corbett RJ. Differences in brain temperature and cerebral blood flow during selective head versus whole-body cooling. Pediatrics. 2001 Nov 1;108(5):1103-10.

## Appendix

### A1: H and E staining

Brain sections obtained from the cryostat were fixed in formalin for 5 min. and rinsed with tap and distilled water for 5 min. each. The sections were dehydrated sequentially in 80%-95%-100% ethanol, soaked in xylene, and rehydrated sequentially in 100%-95%-80% ethanol and finally in distilled water. Then, sections were stained with Harris' hematoxylin (9.3% alum dodecahydrate, 0.46% hematoxylin, 0.046% sodium iodate, 2.8% acetic acid, 4.6% ethanol) for 2 min. and rinsed in distilled water until the water remained colorless. After dipping the sections in acid alcohol (69.7% ethanol, 0.06 M hydrochloric acid), they were immediately washed with distilled water. For bluing, samples were transferred to tap water, rinsed with distilled water, and stained with eosin (0.2% erythrosin B, 0.025% eosin Y, 0.025% eosin B, 0.05% acetic acid, 60% ethanol) before immersion for 2 min. each in 95% and 100% ethanol and xylene. Sections were mounted in Cytoseal 60.

### A2: ELP tagging protocol

The labeling of the ELPs was carried out using Cyanine N-hydroxy succinimide (NHS) ester. The protocol was adapted from the recommended procedure from the manufacturing company, Lumiprobe. The free amino group at the N-terminal of the ELP is allowed to react with the active ester of NHS under an optimal pH range between 8.3 – 8.5 to produce Cy-tagged ELPs. At first, the amount of NHS ester required to label the desired mass of ELP is determined as below:

$$\mathrm{NHS}_{\mathrm{ester}_{\mathrm{weight}}[\mathrm{mg}]} = \frac{8 \times \mathrm{amino\_compound\_weight\ [mg]} \times \mathrm{NHS\_ester\_molar\_weight\ [Da]}}{\mathrm{amino\_compound\_molar\_weight\ [Da]}}$$

8 refers to the experimental value of the molar excess, commonly used for mono-labeling. introOnce the reaction volume was determined, the dye in DMSO constituting about 1/10$^{th}$ reaction volume was mixed with ELP solubilized in 9/10$^{th}$ reaction volume of 0.1 M phosphate buffer at pH ~8.4. The reaction mixture, that was prepared on ice to keep the ELPs below the transition temperature, was then subjected to overnight incubation at 4°C.

The samples were then centrifuged at 14,000g for 10 mins in a temperature-controlled centrifuge at 4C using centrifugal filtration columns with 30 KDa MW cut-off. The retained ELP-containing sample was retrieved by reverse spinning and dialysed overnight against PBS at 4C, to separate the free dye from the tagged ELP. The concentration of the ELP in the final sample was measured to estimate the protein recovery post the tagging process.

Measuring labeling efficiency:

The dye concentration in the tagged ELP sample was determined from the standard curve obtained from plotting the fluorescence values of the standards against their known concentrations. The fluorescence was measured using a fluorescent plate reader set with excitation and emission wavelengths of 646 and 662 nm. The fluorescence of the unknown tagged-ELP samples was then used to calculate the concentration of the dye in the final sample from the equation y=mx+c, where y is the fluorescence of the unknown, x is the concentration and m and c are the slope and intercept values obtained from the standard curve. The labeling efficiency is then calculated from,

Labeling efficiency (%) = $\frac{\mathrm{Tm}-\mathrm{Em}}{\mathrm{Tm}}$ x 100%

Where, Tm is the theoretical moles of dye in the sample assuming 100% labeling efficiency and Em is experimental moles of dye leftover or removed from the sample during the purification process.

**A3: Western blot analysis**

To obtain a strong Western signal, the mass of protein for electrophoresis in each sample represented the maximum amount of total protein that could be obtained uniformly from all lysates of a tissue type. Protein samples were prepared by combining up to 30 µL of lysate supernatant with 10 µL of 4× sample buffer (40% glycerol, 8% sodium dodecyl sulfate, 3.04% Tris, 0.002% bromophenol blue, 8% 2-mercaptoethanol). The samples were loaded onto a polyacrylamide gel (4% stacking gel, 12% separating gel), separated at 100 V for 3 h, and transferred to a polyvinylidene difluoride membrane (Bio-rad, Mississauga, Canada) at 100 V for 1 h. Blots were blocked in 5% milk at room temperature for 1 h and incubated at 4°C overnight in blocking solution containing rabbit primary antibodies (1:1000 dilution) anti-β-Actin, anti-IBA1, anti-cleaved caspase-3, and anti-GFAP. The blot was then incubated for 1h at room temperature with the anti-rabbit secondary antibody conjugated to horseradish peroxidase. TMB Stabilized Substrate for Horseradish Peroxidase (Promega, Madison, USA) was used to develop the blots *via* a color producing reaction.

**A4: Extraction of DEX from tissue using methylene chloride**

The brain divided into left and right hemispheres, was weighed, and homogenized in normal saline (up to 1mL) using a tissue homogenizer. The samples were then subjected to a wash with 5 mL n

heptane in the presence of 1M NaOH (50 µL), in glass centrifuge tubes with Teflon-lined caps. The mixture was kept on a reciprocal shaker for up to 15 minutes. After aspirating the organic layer, 1 µg of internal standard i.e., 10 µL of 0.1 mg/mL prednisolone in methanol, was added to the aqueous phase followed by methylene chloride (5 mL) extraction of the samples. The aqueous layer was then carefully removed, and the remaining organic phase was transferred to another clean glass centrifuge tube. To remove the solvent, samples were dried at 45°C, under a steady stream of nitrogen gas. Tetrahydrofuran (80 µL) was used to reconstitute the sample residue at the time of HPLC analysis. The brain homogenate post methylene chloride extraction and reconstitution in tetrahydrofuran was used as the basis for the preparation of DEX standards at concentrations ranging between 0.1 to 5 µg/mL.